Journal of Medicinal Chemistry

Article

pubs.acs.org/jmc

Discovery and Characterization of MAPK-activated Protein Kinase-2 Prevention of Activation Inhibitors

John G. Cumming,*[,‡] Judit É. Debreczeni,[‡] Fredrik Edfeldt,[†] Emma Evertsson,[†] Martin Harrison,[‡] Geoffrey A. Holdgate,[‡] Michael J. James,[‡] Scott G. Lamont,[‡] Keith Oldham,[‡] Jane E. Sullivan,[‡] and Stuart L. Wells[‡]

[‡]AstraZeneca, Alderley Park, Macclesfield, Cheshire SK10 4TG, United Kingdom

[†]AstraZeneca R&D, Pepparedsleden 1, 431 83 Mölndal, Sweden

Supporting Information

ABSTRACT: Two structurally distinct series of novel, MAPK-activated kinase-2 prevention of activation inhibitors have been discovered by high throughput screening. Preliminary structure−activity relationship (SAR) studies revealed substructural features that influence the selective inhibition of the activation by p38α of the downstream kinase MK2 in preference to an alternative substrate, MSK1. Enzyme kinetics, surface plasmon resonance (SPR), 2D protein NMR, and X-ray crystallography were used to determine the binding mode and the molecular mechanism of action. The compounds bind competitively to the ATP binding site of p38α but unexpectedly with higher affinity in the p38α−MK2 complex compared with p38α alone. This observation is hypothesized to be the origin of the substrate selectivity. The two lead series identified are suitable for further investigation for their potential to treat chronic inflammatory diseases with improved tolerability over previously studied p38α inhibitors.

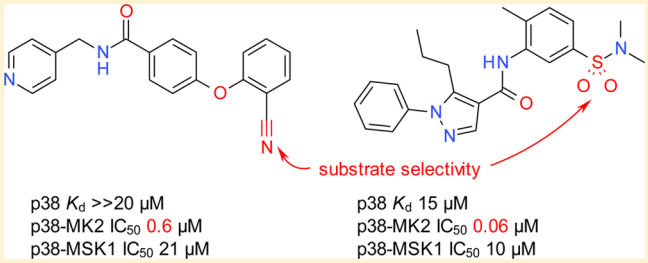

INTRODUCTION

The p38α mitogen-activated protein kinase (MAPK) cellular signaling pathway plays a critical role in the regulation of pro-inflammatory cytokines including tumor necrosis factor α (TNF-α), interleukin-1β (IL-1β), and interleukin-6 (IL-6).[1−3] Biological therapies directed against these cytokines such as etanercept, infliximab, adalimumab, anakinra, and tocilizumab have proven effective in treating autoimmune disease and chronic inflammatory conditions.[4,5] Consequently the development of orally available small molecule alternatives, particularly inhibitors of p38α, has been the goal of a vast amount of research.[6,7] Many potent and selective small molecule inhibitors of p38α with diverse chemotypes have progressed into clinical trials for the treatment of chronic inflammation, but none has yet successfully reached the market, with several advanced compounds failing in Phase II due to adverse events.[8,9] Recently, GlaxoSmithKline reported the initiation of a Phase III trial with losmapimod[10] in acute coronary syndrome; however, clinical development of the compound for rheumatoid arthritis and chronic obstructive pulmonary disease (COPD) appears to have been discontinued. While the area of straightforward inhibition of p38α kinase activity has been thoroughly researched, there remain some interesting, relatively unexplored avenues.[11] For example, CMPD1 (Figure 1) has previously been described as a substrate selective inhibitor of p38α that blocks the p38α-dependent phosphorylation of MAPK-activated protein kinase-2a (MAPKAP-kinase 2a, or MK2a) but not the activation of the transcription factor ATF-2 or the phosphorylation of myelin basic protein (MBP).[12] Kinetic studies demonstrated that CMPD1 is not competitive with ATP, and further studies supported the hypothesis that the inhibitor binds to the docking groove of p38α and prevents its interaction with the carboxy-terminal docking domain of MK2a. However, very little further research on CMPD1 or other substrate selective p38 inhibitors has been published.

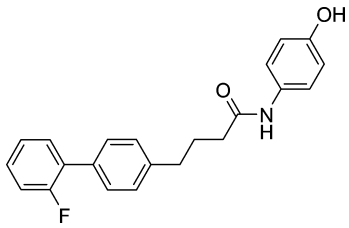

Figure 1. Structure of CMPD1, a substrate-selective p38α inhibitor.

Among the many p38α substrates involved in regulating inflammation MK2 has received the most attention as a potential alternative point of intervention in the p38α signaling pathway. MK2 regulates production of cytokines including TNF-α and IL-6 through a post-transcriptional mechanism, primarily

Special Issue: New Frontiers in Kinases

Received: July 10, 2014

   dx.doi.org/10.1021/jm501038s | J. Med. Chem. XXXX, XXX, XXX−XXX

through modulating the stability and translation of mRNA.[13,14] MK2 knockout mice were shown to be resistant to collagen-induced arthritis, a well-established disease model of rheumatoid arthritis, and also showed a much reduced production of LPS-induced TNF-α, both in vitro and in vivo.[15,16] On the basis of these observations, it has been suggested that a selective MK2 inhibitor might have equivalent clinical efficacy to a p38α inhibitor but reduce or avoid unwanted side effects that may result from interfering with other downstream effects of p38. Small molecule, ATP site binding inhibitors of MK2 have been identified,[17−20] but their cellular potency appears to be limited by unfavorable competition with ATP in the cell, and to date, none has progressed into clinical trials.[21,22] Earlier work at AstraZeneca identified an anilinoquinoline series of MK2 inhibitors that showed mainly uncompetitive behavior with respect to ATP; however the overall profile of the series meant it was unsuitable as a starting point for lead optimization.[23] More recently a novel series of non-ATP competitive MK2 inhibitors has been reported.[24]

Building on experience in these laboratories in exploring alternative kinase inhibition modes, we set out to discover compounds that inhibited the phosphorylation of nonactive MK2 by p38α, acting via a PoA (prevention of activation) mechanism as opposed to the more typical IoC (inhibition of catalysis) mechanism.[25,26] The primary screen is a coupled enzyme assay,[27] in this case measuring the phosphorylation by active p38α of inactive MK2 enzyme, rather than of the artificial substrate MBP, which has been used in the vast majority of historical p38 programs, including our own.[28] The attraction of this approach was its potential to identify novel binding sites or binding modes, avoiding or reducing competition by ATP. Nonactive kinases often have a lower affinity for ATP and lower competition with ATP may reduce the loss of potency often observed in cells due to the high intracellular ATP concentration. MK2 forms a high affinity (K_d = 20 nM) complex with p38α, and it was shown that perturbation of this tight-docking interaction prevents the activation of MK2.[29] This screening strategy is more complex than is typical since the p38α−MK2 coupled enzyme assay requires follow up with a p38α−MBP counter-screen to remove p38α IoC inhibitors. Furthermore, it is important to perform detailed mechanism of action studies in order to elucidate the inhibitor binding site and mode of inhibition.[30]

Hit Finding Strategy. A high throughput screen (HTS) for MK2 PoA inhibitors was developed using ALPHAScreen technology. Three MK2a residues are phosphorylated by p38α at similar rates: Thr222, Ser272, and Thr334.[29] The antibody used in the HTS assay recognizes phosphorylation on Thr222, which is located on the activation loop. The AstraZeneca collection was screened at 10 μM and actives showing >30% inhibition were retested in triplicate. Of the triplicate retest set, 99% of the known inhibitors of p38α−MBP were confirmed as active giving high confidence in the quality of the data. The active compounds were triaged by counter-screening for inhibition of p38α−MBP, and compounds from two structurally distinct series were then selected for further investigation.

CHEMISTRY

Series 1 compounds were synthesized in a very straightforward manner by means of a HATU-mediated amide coupling between readily available 4-aryloxybenzoic acids **1** and readily available primary amines (Scheme 1). The preparation of the initial series 2 compounds **12**−**20** was similarly facile (Scheme 2). Readily available substituted anilines were coupled with either the substituted pyrazole carbonyl chloride **24** or carboxylic acid **25**. Hydrogenolysis of the benzyloxy group gave access to the phenol **15**, while the carboxylic acid **19** was prepared by hydrolysis of the corresponding methyl ester **17**. To explore alternatives to phenyl or 4-chlorophenyl on the pyrazole required the preparation of suitable intermediates (Scheme 3). This was achieved by ring synthesis of the pyrazole from the appropriate hydrazine **26** and enamine **27** to give **28**,[31] followed by trimethylaluminum-mediated amide formation with the readily available aniline **29**. For the synthesis of isobutyl analogue **23**, the sequence was reversed so that amide **30** was synthesized first, with subsequent formation of the enamine **31** and condensation with isobutylhydrazine.

Scheme 1. General Synthesis of Series 1 Compounds (Table 1)[a]

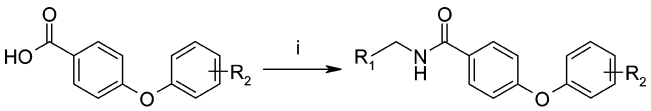

[a]Reagents and conditions: (i) $R_1CH_2NH_2$, HATU, $^iPr_2NEt$, DMF.

RESULTS AND DISCUSSION

Series 1 SAR Studies. Compounds were tested in an ELISA version of the HTS assay for their ability to inhibit the activation of MK2 by phospho-p38α and in an ELISA assay measuring the inhibition of activation of MSK1, an alternative endogenous substrate of p38α. The ratio of the p38α−MK2 and p38α−MSK1 IC_{50} values gives an indication of the substrate selectivity of the inhibitors. The results for compounds in series 1 are shown

Scheme 2. Synthesis of Series 2 Compounds 12−20 (Table 2)[a]

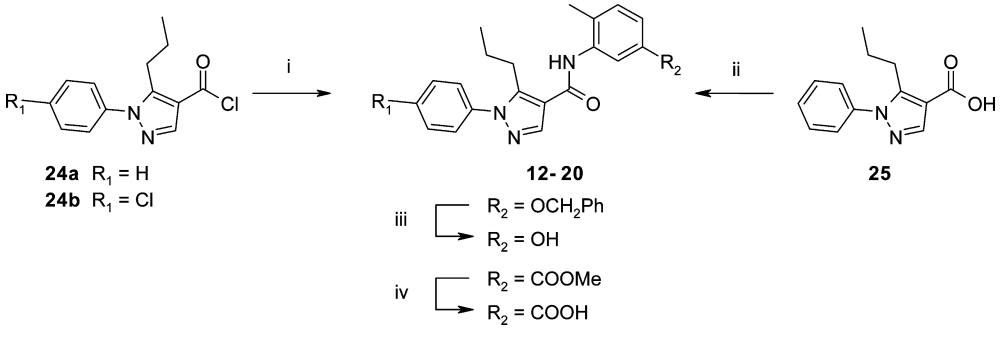

[a]Reagents and conditions: (i) $ArNH_2$, THF; (ii) $ArNH_2$, HATU, $^iPr_2NEt$, DMF; (iii) H_2, Pd/C, EtOH, 40 °C, 5 bar; (iv) 2 M NaOH, THF/MeOH (2:1).

dx.doi.org/10.1021/jm501038s | J. Med. Chem. XXXX, XXX, XXX−XXX

Scheme 3. Synthesis of Series 2 Compounds 21−23 (Table 2)[a]

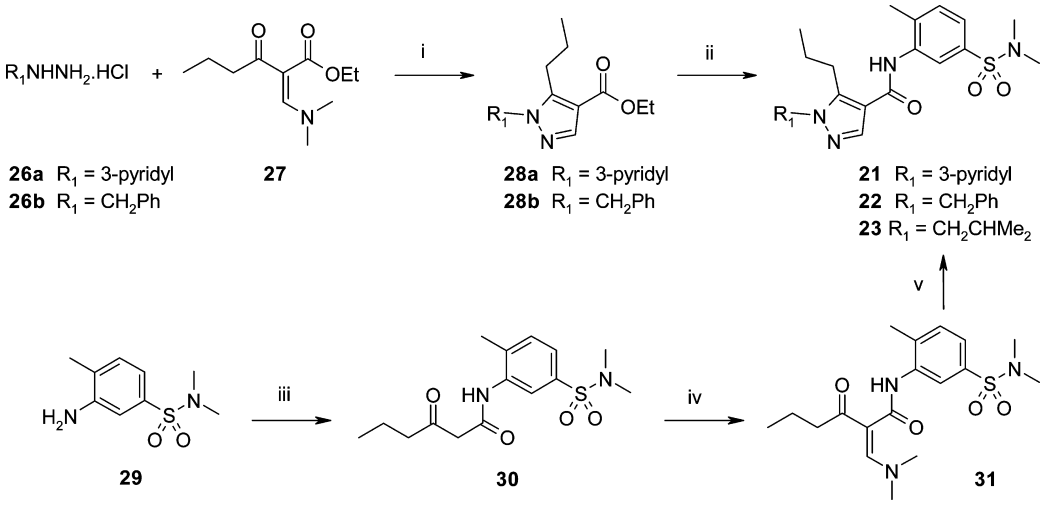

[a]Reagents and conditions: (i) AcOH, EtOH; (ii) **29**, Me_3Al, CH_2Cl_2; (iii) ethyl 3-oxohexanoate, AcOH, 150 °C; (iv) 1,1-dimethoxy-*N*,*N*-dimethylmethylamine, dioxane, 100 °C; (v) isobutylhydrazine hydrochloride, AcOH, EtOH.

in Table 1. All the compounds also gave IC_{50} > 10 μM in the p38α−MBP IoC assay (results not shown). Compounds **2**−**6** (Table 1) were among the cluster emerging from the HTS. The compounds are low micromolar inhibitors with less than 10-fold selectivity with the exception of **6**, which has submicromolar activity and 34-fold selectivity. Compound **6** is also the only one of **2**−**6** with an *ortho*-substituent on the terminal phenoxy group. Compounds **2**−**6** inhibited CYP_{450} 3A4 with IC_{50} values of approximately 1 μM, which is consistent with the presence of a terminal 4-pyridyl group. Compounds **7**−**11** were synthesized in order to explore alternative *ortho*-substituents on the phenoxy and to find replacements of the 4-pyridyl group, which may lead to reduced CYP3A4 inhibition. The results show that replacing 2-cyano with 2-methyl (**7**) or 2-chloro (**8**) gives compounds with a similar profile to compounds **2**−**5** with micromolar potency and minimal selectivity. The 4-pyridyl group in **6** can be replaced with phenyl (**9**) and 3-pyridyl (**10**) with no significant change in potency or selectivity. Replacement with 4-pyrimidinyl (**11**) leads to a small reduction in potency. Compounds **9**, **10**, and **11** were tested for CYP3A4 inhibition, and all showed IC_{50} > 10 μM, confirming that moving away from the 4-pyridyl group does indeed remove this drug metabolism liability.

Series 2 SAR Studies. The results for compounds in series 2 are shown in Table 2. All the compounds also gave IC_{50} > 10 μM in the p38α−MBP IoC assay (results not shown). Compounds **12**−**14** (Table 2) were among the cluster emerging from the HTS. Their potency and substrate selectivity are generally better than the series 1 compounds, with the best compounds **12** and **14** showing <100 nM potency and around 100-fold selectivity. Compounds **15**−**19** were synthesized to investigate changes to the 5-substituent on the amide *N*-phenyl (Table 2). 5-Hydroxy is potent vs both MK2 and MSK1 (**15**), while the bulkier 5-benzyloxy is inactive (**16**). Sulfone or carboxy in the 5-position retained potency and selectivity (**18**, **19**), while the methyl ester analogue **17** showed no selectivity. Next, compounds **20**−**23** were synthesized to examine SAR at the pyrazole *N*-phenyl (Table 2). Addition of a 4-chloro to **12** reduced potency (**20**). The phenyl in **12** could be replaced by benzyl (**22**) or isobutyl (**23**) without significant changes in potency or selectivity. Replacing this phenyl with 3-pyridyl is slightly deleterious to potency but gives a reduction in measured log $D_{7.4}$ of 1.2 units (**21**, log $D_{7.4}$ = 2.3). These preliminary SAR studies indicate that there is scope within both series for further optimization of potency and drug-like properties while retaining the high levels of substrate selectivity.

Further Profiling of the Series. Representative compounds from both series were tested for their ability to inhibit p38α-mediated signaling in cells as measured by inhibition of LPS-stimulated TNF-α production in human PBMCs and of IL-1-stimulated PGE_2 release in TC28 cells. The series 1 compounds tested generally showed low micromolar potency in both assays (Table 3). Series 2 compounds **12** and **14** were also active in cells with submicromolar potency being achieved for **14** in TC28 cells; however compound **19** showed a much reduced potency in cells, likely attributable to poor cellular permeability arising from the carboxylic acid group. To assess general kinase selectivity, compounds **6** and **12** were tested in a panel of 50 protein kinases at 10 μM and showed <25% inhibition against all with the exception of p38α and IGF1R (30% to 45% inhibition). Physicochemical properties and in vitro metabolic stability were generally favorable for series 1 compounds (Table 4), while the initial series 2 compounds had rather low solubility and high plasma protein binding. The data for the later compound **21** shows that by reduction of lipophilicity there is scope for improving these properties. The in vitro metabolic stability was variable for the series 2 compounds indicating this is an aspect that requires monitoring during subsequent optimization.

Mechanism of Action Studies. A combination of biochemical and biophysical approaches together with X-ray crystallography were employed to probe the mechanism of action and the binding site of representative compounds in order to elucidate the binding mode of these novel MK2 PoA inhibitors.

Competition Experiments. Biochemical competition experiments were performed to establish whether the compounds were competitive, noncompetitive, or uncompetitive with respect to both ATP and MK2 in the p38α−MK2 phosphorylation reaction. The concentration−rate curves for compounds **6** and **12** with varying concentrations of ATP are shown in Figure 2. The data were fit to the standard equations for competitive, noncompetitive, uncompetitive, and mixed competitive mechanisms. The best fit was to the competitive mechanism for both compounds, and the calculated K_i values were 0.29 ± 0.046 μM

dx.doi.org/10.1021/jm501038s | J. Med. Chem. XXXX, XXX, XXX−XXX

Table 1. Activity Data for Series 1 Compounds

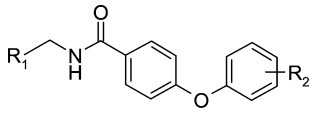

Compound	R_1	R_2	p38α-MK2 IC_{50} (μM)[a]	p38α-MSK1 IC_{50} (μM)[a]	Substrate selectivity
2	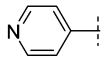	H	2.3	4.0	1.7
3	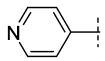	4-Me	4.7	22	4.7
4	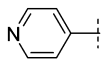	4-Cl	2.4	10	4.2
5	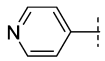	4-F	2.1	2.3	1.1
6	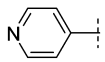	2-CN	0.60	21	34
7	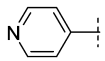	2-Me	2.0	5.4	2.7
8	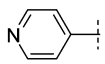	2-Cl	1.7	1.7	1.0
9	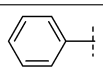	2-CN	0.45	>100	>220
10	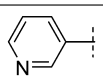	2-CN	0.56	15	27
11	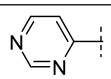	2-CN	2.8	>100	>36

[a]IC_{50} data are the geometric mean of at least three independent measurements, the SEM of which is within 2-fold, unless otherwise stated.

for compound **6** and 0.014 ± 0.0023 μM for compound **12**, which are in good agreement with their IC_{50} values in the p38α–MK2 assay.

SPR Studies. The affinity of the compounds for binding to phosphorylated p38α was determined by an inhibition in solution (ISA) assay[32] using surface plasmon resonance (SPR) with an ATP-site-binding small molecule as the immobilized target definition compound (TDC). Series 1 compound **6** showed 17% displacement of the TDC at 20 μM, which implies that its binding affinity constant (K_d) is much greater than 20 μM. Series 2 compound **12** had a K_d value of 15.4 μM determined by this method (log K_d = 1.19 ± 0.03). For both compounds, the K_d value for binding to phosphorylated p38α is far higher than the IC_{50} in the p38α–-MK2 enzyme assay (at least 100-fold for **6** and 250-fold for **12**), suggesting an increased affinity for the phospho-p38α–MK2 complex compared with binding to phospho-p38α alone.

Two-Dimensional Protein NMR Studies. Protein-observed 2D NMR is a technique that can detect both weak and tighter binding of ligands to proteins in solution and, in some cases, can give an insight into the location of the binding site by examination of the amino acid residues that shift upon ligand binding. Four systems were used to investigate the binding of compounds to p38α and MK2 alone and together in the complex: $^{2}H,^{15}N$-labeled p38α and $^{2}H,^{15}N$-labeled MK2 for studying the free proteins, $^{2}H,^{15}N$-labeled p38α and unlabeled MK2 to study p38α in the complex, and $^{2}H,^{15}N$-labeled MK2 and ^{2}H-labeled p38α to study MK2 in the complex (phosphorylated full length p38α and a construct of MK2 containing residues 46–400 were used in each case). Compounds **6** (series 1) and **12** (series 2) showed either no binding or weak binding (around 50 μM for free p38α with **6**) to either of the free enzymes. However, **6** clearly demonstrated effects on residues in both p38α and MK2 in the complex. The observed effects were generally consistent with intermediate ligand-exchange on the NMR time scale, which suggests binding in the low micromolar range. The observed chemical shift changes were similar to those seen in the free form of p38α and were suggestive of an interaction in the ATP site; however, in general it is difficult to pinpoint the site of binding for compounds in p38α using NMR even for known p38α ATP-site

dx.doi.org/10.1021/jm501038s | J. Med. Chem. XXXX, XXX, XXX–XXX

Table 2. Activity Data for Series 2 Compounds

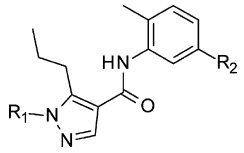

Compound	R_1	R_2	p38α-MK2 IC_{50} (μM)[a]	p38α-MSK1 IC_{50} (μM)[a]	Substrate selectivity
12		SO_2NMe_2	0.061	9.7	160
13		F	0.11	2.5	23
14		CN	0.015[b]	0.89	60
15		OH	<0.046[b]	<0.046[b]	-
16		OCH_2Ph	>100[b]	>100[b]	-
17		CO_2Me	0.49	0.50	1.0
18		SO_2Me	0.19	23	120
19		CO_2H	0.086	4.2	49
20	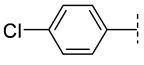	SO_2NMe_2	0.39	20	50
21		SO_2NMe_2	0.27	>30	>110
22	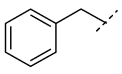	SO_2NMe_2	0.053	6.3	120
23	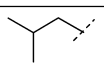	SO_2NMe_2	0.076	5.4[b]	72

[a] IC_{50} data are geometric mean of at least three independent measurements, the SEM of which is within 2-fold, unless otherwise stated. [b] $n = 2$.

binders. Compound **12** showed weak binding to p38α in the complex with similar chemical shifts to those seen for compound **6**, but effects were observed on MK2 residues in the complex, consistent with tight binding (nanomolar affinity) and slow ligand-exchange on the NMR time scale. There were many small shifts upon ligand binding throughout the protein (Figure 3); the largest changes were in the ATP-site (Cys140, Asp207, and Phe208), a loop near the ATP-site but away from p38α (Gly154 and Asp155), and one residue at the interface between MK2 and p38α (Lys307). Phosphorylation of p38α is not important for binding of these compounds; results with the nonphosphorylated p38α–MK2 complex were essentially same as those with the phosphorylated p38α–MK2 complex (results not shown). Comparison between the NMR spectra of free p38α and p38α in the complex reveals that only minor structural changes occur in p38 upon complex formation. However, from comparison of the NMR spectra of free MK2 and MK2 in the complex, it is clear that MK2 undergoes a major conformational change upon

dx.doi.org/10.1021/jm501038s | J. Med. Chem. XXXX, XXX, XXX–XXX

Table 3. Cellular Activity Data for Selected Compounds

compd	series	hPBMC LPS-TNF-α[a] (μM)	TC28 IL-1-PGE$_2$ (μM)[a]
6	1	6.1, 5.4	25,25
9	1	*b*	1.4[c]
10	1	*b*	4.7[c]
11	1	*b*	7.1[c]
12	2	1.5	0.97
14	2	*b*	0.21, 0.30
19	2	21	*b*

[a]IC_{50} data are the geometric mean of at least three independent measurements, the SEM of which is within 1.5-fold, unless otherwise stated where individual results are shown. [b]Not determined. [c]n = 1.

MK2−p38α complex formation. Unstructured parts of MK2, such as the C-terminal tail, become more rigid and structured, which is consistent with the findings from our own (vide infra) and published X-ray crystallographic studies of the p38α−MK2 complex.[33,34]

X-ray Crystallographic Studies. X-ray crystal structures of the unphosphorylated p38α−MK2 heterodimer in complex with series 1 compound **6** and series 2 compound **12** were determined to 2.3 and 3.0 Å, respectively.[35] The ligands are bound at the ATP site of p38α in both structures, which is consistent with the observation that both series are competitive with ATP. They both have hydrogen bonding interactions with the hinge Met109 N−H (the amide carbonyl in **6** and the unsubstituted pyrazole nitrogen in **12**) and with Asp168 N−H (nitrile group in **6** and a sulfonyl oxygen in **12**) in the DFG loop (Figure 4). The distal phenyl ring of the diphenylether in **6** and the methyl group in **12** are buried in the hydrophobic "selectivity" pocket formed by residues Lys53 and Thr106. The structure with **6** shows a secondary ligand binding site in the C-terminal lobe of p38α in a shallow pocket enclosed by p38α residues 190−195, 250−258, and 290−295. There are no specific interactions with the ligand, and it is probable that this binding mode is a crystallization artifact. From the overlay between the two structures, it can be seen that the substituents that were found from the SAR studies to be critical for potency and substrate selectivity, namely, the 2-cyano in **6** and 5-sulfonamido in **12**, occupy the same space in the binding site and make the same interaction with the protein. Moreover, the series 2 SAR indicates that sulfonamido can be replaced with cyano (compound **14**, Table 2) with retention of potency and substrate selectivity.

The protein structures of the ligand-bound p38α−MK2 complexes are in very good agreement with the previously published apo structures 2ONL (4.0 Å) and 2OZA (2.7 Å). Interestingly, in the complex with **12** the entire C-terminal α helix of MK2 (Pro381′−His400′) is well ordered, whereas the terminal 7−10 residues are disordered in the complex with **6** and the published apo structures.

X-ray crystal structures of p38α inhibitors **32** (Locus Pharmaceuticals[36]) and **33** (Bristol-Myers Squibb[37]) (Figure 5) bound to p38α are available for comparison with the herein published complex structures and show small but distinct changes. In Figures 6 and 7, amino acids Leu104 to Leu108, which includes the hinge, have been overlaid using MOE.[38] Not surprisingly there are changes in the p38α amino acids close to the MK2 surface introduced by the direct interaction between the proteins, such as Asn114 and Asn115, which are in the ligand binding pocket. The changes in p38α induced by binding of MK2 are transferred through the protein and conformational changes can be seen all the way to Glu71, which is more than 12 Å away from the MK2−p38α interface. Although all the structures show a DFG-in conformation, the ring orientation of Phe169 of the DFG loop shows a perpendicular orientation in the complex structures compared with the p38α alone structures, and also Asp168 shows a different conformation in the MK2−p38α complex structures (Figure 6). These various changes should make it possible to design further compounds such as those in series 1 and 2, which, although structurally similar to p38α

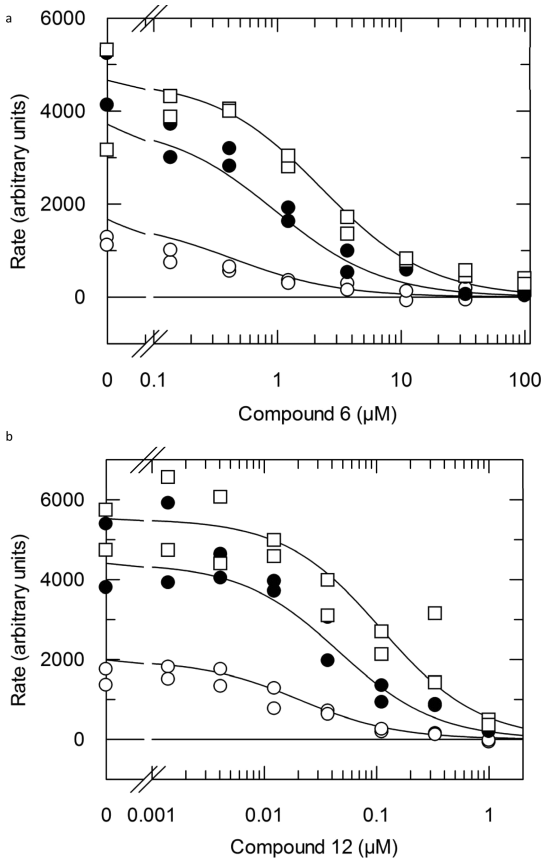

Figure 2. Concentration−rate curves for the p38α−MK2 assay at varying concentrations of ATP in the presence of (a) compound **6** or (b) compound **12**. ATP concentrations: (○) 40, (●) 200, or (□) 600 μM.

Table 4. Physicochemical and In Vitro PK Data for Selected Compounds

compd	series	solubility (μM)[a]	PPB (% free) (R/H)[b]	human Mics[c] CL$_{int}$ (μL/(min·mg))	rat Heps[d] CL$_{int}$ (μL/(min·10^6 cells))
6	1	120	14/8.5	<2	28
11	1	360	20/27	<2	23
12	2	0.55	3.1/2.3	62	42
21	2	21	24/26	143	10

[a]Aqueous solubility was measured under thermodynamic conditions at pH 7.4. [b]Plasma protein binding (PPB) was assessed by equilibrium dialysis in the appropriate species (rat/human) at 37 °C. Free and bound concentrations were determined by LC-MS. [c]Human microsomes. [d]Rat hepatocytes.

dx.doi.org/10.1021/jm501038s | J. Med. Chem. XXXX, XXX, XXX−XXX

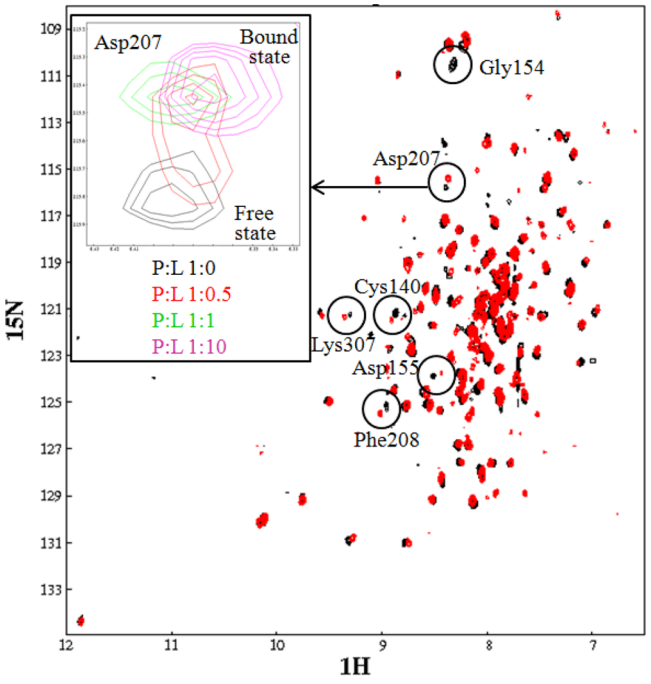

Figure 3. Two-dimensional NMR TROSY-HSQC spectra of $^{2}H,^{15}N$-labeled MK2−^{2}H-labeled p38α complex in the absence (black) and presence of **12** (red). Assigned residues exhibiting the largest chemical shift changes are indicated. The inset shows the titration of **12** for the peak corresponding to Asp207, with the protein (P) to ligand (L) ratios indicated. Slow exchange is evident from the appearance of two peaks, corresponding to the ligand-free and ligand-bound state, at 0.5 equiv of **12**.

binders, selectively target the MK2−p38α complex, showing limited binding to the p38α in the absence of MK2.

CONCLUSIONS

Using a coupled enzyme HTS followed by counter-screening with an artificial substrate enzyme assay, we discovered two distinct hit series of selective inhibitors of the activation of MK2 by p38α. SAR studies revealed the critical substitutions that are required for the p38α substrate selectivity and that differentiate these compounds from previously reported p38α inhibitors based on the same structural templates. Kinetic studies revealed that the compounds are competitive with ATP, with K_i values close to the IC_{50} in the coupled enzyme assay. X-ray crystallography confirmed that the compounds bind in the ATP binding site of p38α in the p38α−MK2 complex and examination of overlays with published crystal structures showed very high structural similarity with the p38α−MK2 apo crystal structures and small but distinct differences with structures of structurally related ligands bound to p38α alone. SPR and 2D protein NMR studies showed that the compounds have weak or insignificant binding to phosphorylated p38α in the absence of MK2, which is consistent with the observed substrate selectivity. Two-dimensional protein NMR of the p38α−MK2 complex showed increased ligand binding affinities consistent with their level of activity in the coupled enzyme assay. Ligand binding led to shifts in the MK2 protein residues in the complex, remote from the ligand binding site.

The two series showed inhibition of the p38α pathway in cells and had promising lead-like properties suitable for further optimization. The X-ray crystal structures provide opportunities to design compounds with improved potency and substrate selectivity. To the best of our knowledge, this work represents the first report of compounds that bind to the ATP binding site of a protein kinase and are competitive with ATP but, unexpectedly, show selectivity for inhibiting the phosphorylation of one substrate of the kinase over another. Our data suggest that this effect is due to an increased ligand binding affinity for the

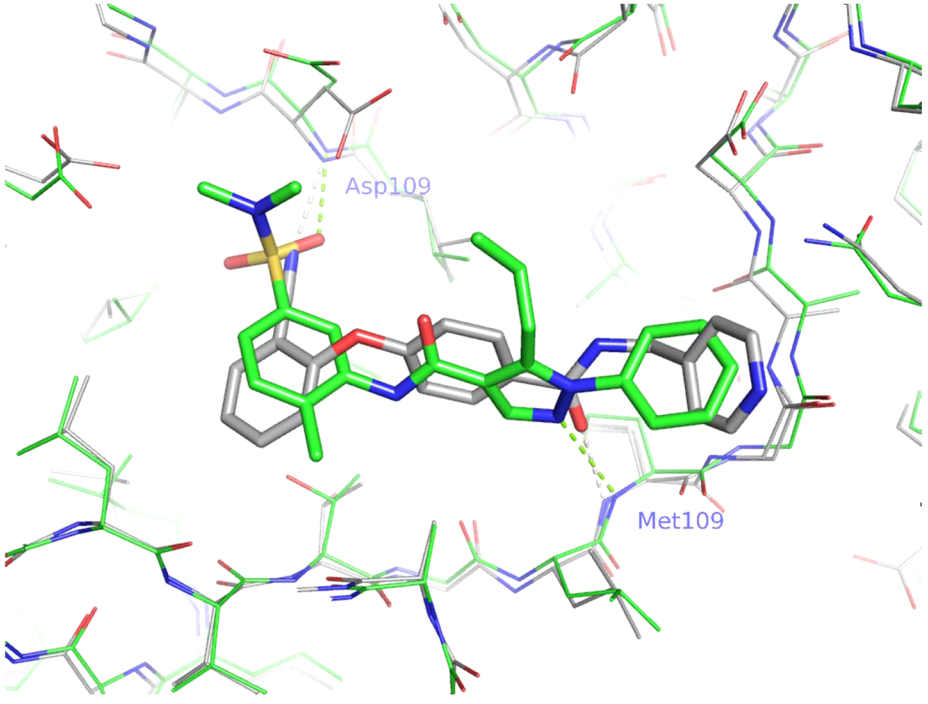

Figure 4. Overlay of p38α−MK2 ternary complex structures with compounds **6** (gray) and **12** (green). Dashed lines indicate H-bonding interactions between the ligands and protein residues.

dx.doi.org/10.1021/jm501038s | J. Med. Chem. XXXX, XXX, XXX−XXX

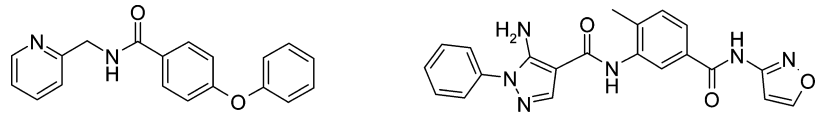

32 33

Figure 5. Literature p38α inhibitors that bind to the ATP binding site.

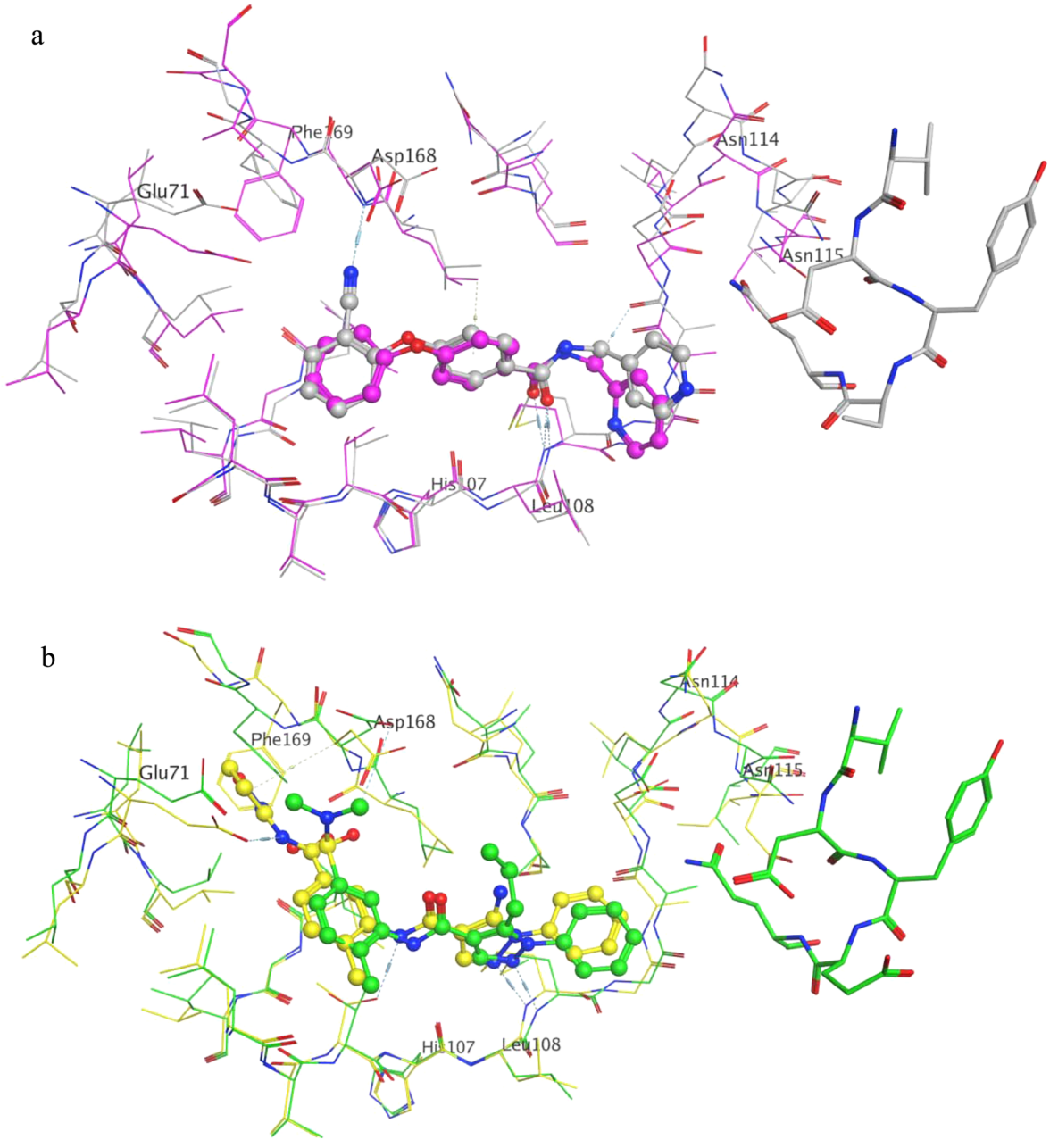

Figure 6. Overlays of the ligand binding regions of compounds in the present study with published structures of structurally similar p38α ligands. Amino acids belonging to MK2 are indicated with bold sticks. (a) Compound **6** bound to the p38α–MK2 complex structure (gray, PDB code 4TYK) and compound **32** bound to p38α (purple, PDB code 1ZYJ); (b) compound **12** bound to the p38α–MK2 complex structure (green, PDB code 4TYH) and compound **33** bound to p38α (yellow, PDB code 3OCG).

kinase–kinase complex relative to the isolated kinase. One can speculate whether this observation is peculiar to the p38α–MK2 system or whether similar ATP-competitive, substrate selective inhibitors might be found for other protein kinases. Further optimization of series 1 and 2 compounds together with detailed studies of their ability to selectively inhibit alternative signaling pathways downstream of p38α in cells will be reported in due course.

EXPERIMENTAL SECTION

Biochemical and Cellular Activity Assays. Compounds were tested at a range of concentrations. The mean data values for each

dx.doi.org/10.1021/jm501038s | J. Med. Chem. XXXX, XXX, XXX–XXX

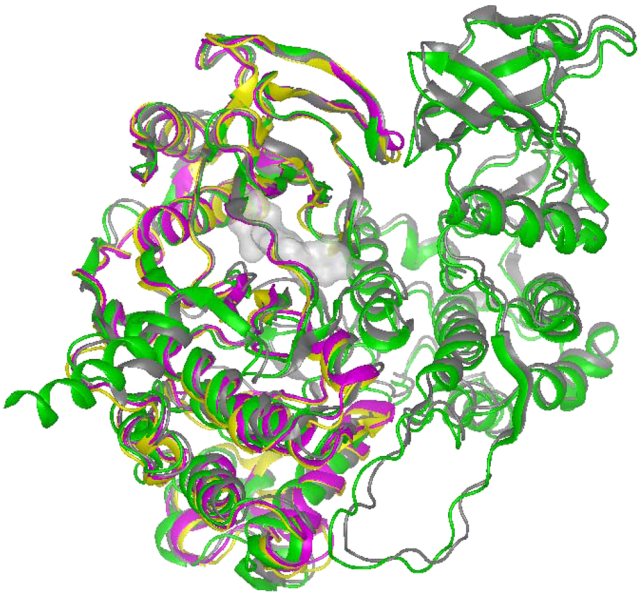

Figure 7. This shows the overall differences in the protein structures. All structures have been overlaid on the hinge region using the MOE software.[38] p38α–MK2 complex structures in gray (compound **6**) and green (compound **12**) and p38α structures in purple (PDB code 1ZYJ) and yellow (PDB code 3OCG). The ligand binding pocket is shown as a gray surface.

concentration along with untreated control wells and 100% inhibition or competition control wells were used to derive a plot of inhibition or competition against concentration. Origin software was used to interpolate the IC_{50} values by nonlinear regression.

p38α-MK2 Inhibition Assay. The inhibitory activity of compounds against the phosphorylation of MK2 by p38α was determined by ELISA. The kinase reaction takes place as a homogeneous assay in solution. Recombinant 5′-c-myc, 6His-tagged human p38α is activated prior to use by incubation with recombinant GST-tagged MKK6 for 3 h at 30 °C; then it is used to phosphorylate Avi, 6His tagged recombinant human MK2[46–400] substrate. Phosphorylated MK2 is then captured by using a NeutrAvidin coated ELISA plate and detected with a rabbit antibody directed toward the phosphorylated site (Thr222) of MK2. Compounds were serially diluted in 100% (v/v) DMSO before being transferred into 384 well assay plates. Kinase activity assays were performed in a total reaction volume of 24 μL. The assay buffer consisted of 50 mM MOPS, 10 mM $MgCl_2$, 1 mM DTT, and 0.01% Tween 20. A 12 μL enzyme mix consisted of 0.1 nM phospho-p38α and 200 μM ATP in assay buffer. A 6 μL substrate mix consisted of 160 nM MK2 in assay buffer. A 6 μL compound mix consisted of the test compound and 4% DMSO in assay buffer. Following a 60 min incubation, 25 μL of stop mix, which consisted of 50 mM EDTA in water, was added. The kinase reaction (10 μL) was transferred to a NeutrAvidin coated ELISA plate and incubated successively with 30 μL ELISA buffer for 1.5 h, with 40 μL of a solution of phospho-MK2 antibody (5 μL in 20 mL TBST, 0.1% BSA) for 1 h and with 40 μL of a solution of goat anti-rabbit HRP (5 μL in 20 mL TBST, 0.1% BSA) for 1 h. QuantaBlu solution (40 μL) was added, and the plate was read on the Pherastar plate reader. Rabbit phospho-MK2 (Thr222) antibody and goat-anti-rabbit HRP were obtained from New England BioLabs (Cell Signalling Ab's).

p38α-MSK1 Inhibition Assay. The assay was performed exactly as for the p38α-MK2 inhibition assay, using recombinant human MSK1 substrate instead of MK2 and anti-phospho-MSK1 antibody instead of anti-phospho-MK2 antibody.

hPBMC Assay. The ability of compounds to inhibit TNF-α production was assessed by using human peripheral blood mononuclear cells (PBMCs), which synthesize and secrete TNF-α when stimulated with lipopolysaccharide (LPS). PBMCs were isolated from heparinized (l0 units/mL heparin) human blood by density centrifugation (in a Sorval RT6000B centrifuge). Mononuclear cells were resuspended in culture medium [RPMI 1640 medium (Gibco) supplemented with 50 units/mL penicillin, 50 μg/mL streptomycin, 2 mM L-glutamine, and 1% heat-inactivated human AB serum (Sigma H-1513)]. Compounds were solubilized in DMSO at a concentration of 10 mM and diluted 1:50 in culture medium, and subsequently serial dilutions were made in culture medium containing 0.5% DMSO. PBMCs (2.6×10^5 cells in 100 μL culture medium) were incubated with 50 μL of culture medium containing 0.5% DMSO for 30 min in 96 well flat-bottom tissue culture plates. Lipopolysaccharide [LPS *Escherichia coli* 0111:B4 (Sigma L-4130), 50 μL, final concentration 0.1 μg/mL] solubilized in culture medium was added to appropriate wells. Culture medium (20 μL) was added to "medium alone" control wells. Six "LPS alone" and four "medium alone" controls were included on each 96 well plate. Plates were incubated for 7 h at 37 °C after which 150 μL of the supernatant was removed from each well and stored at −20 °C. TNF-α levels were determined in each sample using a human TNF-α ELISA.

TC28 Assay. The ability of compounds to inhibit PGE_2 release was assessed by using cells from the human chondrocyte cell line TC28, which synthesize and secrete PGE_2 when stimulated with IL-1. TC28 cells from an in-house tissue culture were seeded at 3×10^4 cells/well into 96 well flat bottomed tissue culture plates. The cells were incubated at 37 °C overnight to allow the cells to attach. Compounds were solubilized in DMSO at a concentration of 10 mM, and serial dilutions were performed in neat DMSO. Compound solution (10 μL) in DMSO (or neat DMSO for assay control wells) was transferred to 790 μL of assay medium [DMEM (Sigma D6546) supplemented with 1% heat inactivated FCS, 1% L-glutamine (Invitrogen), 50 IU/mL penicillin, 50 μg/mL streptomycin (Invitrogen), and 1% nonessential amino acids (Invitrogen)]. The cells were incubated with compound or DMSO control at 37 °C for 20 min. IL-1β (100 μL, R&D systems) at 0.125 ng/mL in sterile PBS+0.1% FCS was added to each well, and the plates incubated at 37 °C for 24 h. The assay medium was transferred into round-bottom 96 well plates, and the plates were stored at −20 °C. The PGE_2 levels were determined in each sample using a PGE_2 ELISA.

Inhibition in Solution Assays (ISAs). These were carried out on a BIAcore 3000 instrument. An inhibitor (1-[7-[3-[4-(aminomethyl)-1-piperidyl]propoxy]-6-methoxy-quinazolin-4-yl]-3-(2-chloro-6-methylphenyl)urea[39]) was immobilized onto a CM-5 sensor chip using standard amine coupling procedures.

The test compound competes for kinase binding to the immobilized inhibitor, resulting in a signal proportional to the free protein concentration. The chip was calibrated using a report point of 50 s. ISAs were carried out with a flow rate of 20 μL/min in HBS-EP ((10 mM HEPES, 150 mM NaCl, 3 mM EDTA, 0.005% Tween-20) buffer containing 0.5% DMSO. GST-tagged phosphorylated p38α was used at 50 nM. Surface regeneration between each injection was carried out with 0.5% sodium dodecyl sulfate for 30 s. Dose–response data were analyzed by nonlinear regression with GraFit (Erithacus Software Ltd.) to estimate K_d values by a standard dose–response equation (eq 1) if $K_d \gg [p38\alpha]$ or a dose–response equation that took into account tight binding of the inhibitor to the protein (eq 2) if K_d was not $\gg[p38\alpha]$.

$$RU = RU_{max}/(1 + [I]/K_d) + b \quad (1)$$

$$RU = (RU_{max}/2)\left(1 - K_d/[p38\alpha] - [I]/[p38\alpha] + \sqrt{(K_d/[p38\alpha] + [I]/[p38\alpha] - 1)^2 + 4K_d/[p38\alpha]}\right) + b \quad (2)$$

Two-Dimensional Protein NMR. Proteins for NMR studies were expressed in *E. coli* and purified using NiNTA affinity chromatography followed by gel-filtration chromatography. $^2H,^{15}N$-labeled p38α and $^2H,^{15}N$-labeled MK2 were produced using ready-to-use Spectra 9 DN minimal medium (Cambridge Isotope Laboratories), ^2H-labeled p38α was produced using Spectra 9 D, and unlabeled MK2 was produced using regular LB medium. The p38α–MK2 complexes were formed by mixing equimolar amounts of the appropriate protein variants. However, a subsequent gel-filtration step proved essential for high spectral quality. Buffer conditions for the NMR studies were 50 mM HEPES, pH 7.5, for the complex, 50 mM MES, pH 6.2, for free MK2,

dx.doi.org/10.1021/jm501038s | J. Med. Chem. XXXX, XXX, XXX–XXX

and 50 mM Tris, pH 7.5, for free p38α, each containing 2 mM reducing agent (TCEP). Typical NMR samples contained 50−100 μM protein. Two-dimensional NMR TROSY-HSQC titration experiments were carried out on a Bruker 800 MHz spectrometer. Backbone assignments were adapted from previous in-house work on MK2[40] and from the literature for p38α.[41] Most assignments from the free proteins could readily be transferred to the complex, since shifts were generally modest.

X-ray Crystal Structures. Murine p38α and human MK2 protein samples were prepared following the protocol described by White et al.[34] These were combined in an equimolar ratio and concentrated to 8 mg/mL. Crystals were obtained using the hanging drop method at room temperature with 9% PEG4000 or 8% PEG3350 and 100 mM sodium citrate at pH 5.6 as precipitants. Compounds were introduced at the crystallization stage. Co-crystallization of compounds was performed using 100 mM DMSO stock solutions of compounds added to the protein solution at 0.5−3 mM prior to crystallization. Crystals were flash-frozen for data collection using 20% glycerol as cryoprotectant. Diffraction images were collected at 100 K at the ESRF beamlines ID23-1 and ID29. Data were processed and the structures were solved using the *CCP4* software suite.[42] Models were built with Coot[43] and refined with *refmac5*.[44] Data collection and refinement statistics are summarized in Table 5 in the Supporting Information.

Synthesis and Characterization of Compounds. *General Chemistry Statement.* All solvents and chemicals used were reagent-grade. Purity and characterization of compounds were established by a combination of LC-MS and NMR. LC-MS spectra were obtained by use of a Waters liquid chromatography mass spectrometry system, where purity was determined by UV absorption at a wavelength of 254 nm or 220−300 nm, and the mass ion was determined by electrospray ionization (Micromass instrument). All test compounds were >95% purity as assessed by LC-MS and ^{1}H NMR. ^{1}H and ^{13}C NMR spectra were recorded on a Varian AV400 FT spectrometer or on a Bruker AV700 spectrometer, in deuterated dimethyl sulfoxide (DMSO-d_6) or $CDCl_3$, with the data expressed as chemical shifts in parts per million (ppm) and are measured relative to the internal residual solvent peak ($CDCl_3$ 7.25 ppm/77 ppm). Preparative HPLC was performed on a Waters or Phenomenex column with decreasingly polar mixtures of water (containing 1% formic acid or 1% aqueous NH_4OH) and MeCN.

*4-(2-Cyanophenoxy)-N-(pyridin-4-ylmethyl)benzamide (**6**).*

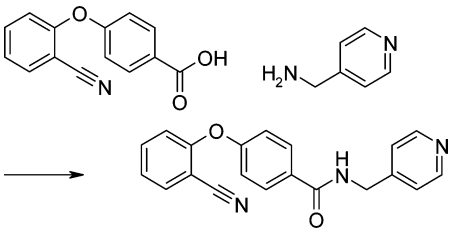

A solution of 4-(2-cyanophenoxy)benzoic acid (100 mg, 0.42 mmol) and HATU (160 mg, 0.42 mmol) was allowed to stir at room temperature for 5 min before adding 4-aminomethylpyridine (43 mg, 0.40 mmol) and DIPEA (350 μL, 2.0 mmol). This solution was allowed to stir at room temperature overnight. The reaction mixture was diluted with acetonitrile (1 mL), water (2 mL), and ammonium hydroxide (0.5 mL) before purifying by reverse phase base (NH_4OH) modified preparative HPLC. Pure fractions were combined and evaporated before being lyophilized (freeze-dried) overnight. There was thus obtained 4-(2-cyanophenoxy)-*N*-(pyridin-4-ylmethyl)benzamide (110 mg, 80%) as a white solid. ^{1}H NMR (400.13 MHz, DMSO-d_6) δ 4.51 (2H, d, J = 5.9 Hz), 7.13 (1H, d, J = 7.8 Hz), 7.23 (2H, d, J = 9.0 Hz), 7.32 (2H, d, J = 6.8 Hz), 7.36−7.40 (1H, m), 7.71−7.76 (1H, m), 7.95−7.97 (1H, m), 8.01 (2H, d, J = 9.0 Hz), 8.51−8.52 (2H, m), 9.18 (1H, t, J = 5.9 Hz); ^{13}C NMR (176 MHz, DMSO-d_6, 30 °C) 42.7, 103.6, 115.6, 118.4, 118.9, 122.0, 124.6, 129.7, 130.2, 134.3, 135.4, 148.5, 149.4, 157.6, 157.8, 165.5; ESI$^+$ m/z (M + H)$^+$ 330.32; ESI-HRMS calculated for $C_{20}H_{15}N_3O_2$ (M + H$^+$) 330.1243; found, 330.1267.

*4-(2-Methylphenoxy)-N-(pyridin-4-ylmethyl)benzamide (**7**).*

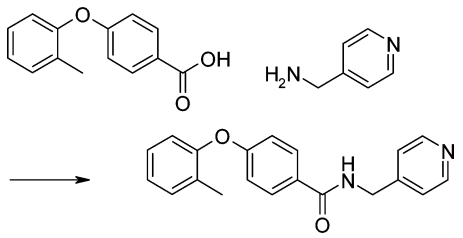

A solution of 4-(2-methylphenoxy)benzoic acid (36 mg, 0.16 mmol) and HATU (60 mg, 0.16 mmol) in DMF (1.5 mL) was allowed to stir at room temperature for 5 min before adding 4-aminomethylpyridine (16 mg, 0.15 mmol) and DIPEA (130 μL, 0.75 mmol). This solution was allowed to stir at room temperature overnight. The reaction mixture was diluted with acetonitrile (1 mL), water (2 mL), and ammonium hydroxide (0.5 mL) before purifying by reverse phase base (NH_4OH) modified preparative HPLC. Pure fractions were combined and evaporated before being lyophilized (freeze-dried) overnight. 4-(2-Methylphenoxy)-*N*-(pyridin-3-ylmethyl)benzamide (23 mg, 44%) was thus obtained as a gum. ^{1}H NMR (400.13 MHz, DMSO-d_6) δ 2.15 (3H, s), 4.49 (2H, d, J = 5.8 Hz), 6.91−6.95 (2H, m), 7.01−7.03 (1H, m), 7.17−7.21 (1H, m), 7.26−7.30 (3H, m), 7.36−7.40 (1H, m), 7.90−7.93 (2H, m), 8.49−8.51 (2H, m), 9.06 (1H, t, J = 5.8 Hz); ESI$^+$ m/z (M + H)$^+$ 319.

*4-(2-Chlorophenoxy)-N-(pyridin-4-ylmethyl)benzamide (**8**).*

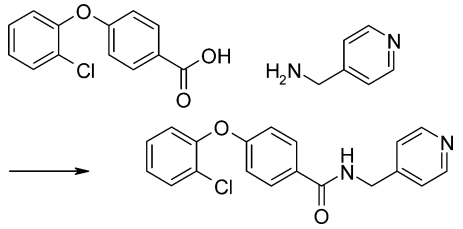

A solution of 4-(2-chlorophenoxy)benzoic acid (20 mg, 0.08 mmol) and HATU (31 mg, 0.08 mmol) in DMF (1.5 mL) was allowed to stir at room temperature for 5 min before adding 4-aminomethylpyridine (8 mg, 0.08 mmol) and DIPEA (66 μL, 0.38 mmol). This solution was allowed to stir at room temperature overnight. The reaction mixture was diluted with acetonitrile (1 mL), water (2 mL) and ammonium hydroxide (0.5 mL) before purifying by reverse phase base (NH_4OH) modified preparative HPLC. Pure fractions were combined and evaporated before being lyophilized (freeze-dried) overnight. There was thus obtained 4-(2-chlorophenoxy)-*N*-(pyridin-4-ylmethyl)benzamide (16 mg, 44%) as an amber gum. ^{1}H NMR (400.13 MHz, DMSO-d_6) δ 4.49 (2H, d, J = 5.8 Hz), 6.99−7.01 (2H, m), 7.24−7.33 (4H, m), 7.42−7.46 (1H, m), 7.64−7.67 (1H, m), 7.93−7.95 (2H, m), 8.50 (2H, m), 9.10 (1H, t, J = 5.8 Hz); ESI$^+$ m/z (M + H)$^+$ 339.

*N-Benzyl-4-(2-cyanophenoxy)benzamide (**9**).*

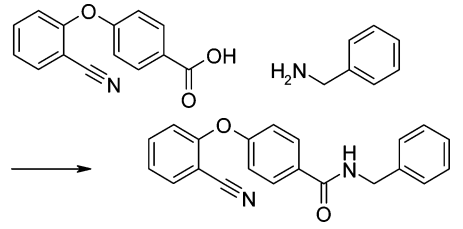

A solution of 4-(2-cyanophenoxy)benzoic acid (97 mg, 0.41 mmol) and HATU (185 mg, 0.49 mmol) in DMF (2 mL) was allowed to stir at room temperature for 5 min before adding benzylamine (0.049 μL, 0.45 mmol) and DIPEA (0.21 μL, 1.2 mmol). This solution was allowed to stir at room temperature overnight. The reaction mixture was diluted to 5 mL with acetonitrile/water and purified by preparative HPLC (Waters XTerra C18 column, 5 μm silica, 19 mm diameter, 100 mm length, 254 nm), using decreasingly polar mixtures of water (containing 0.1% NH_3) and MeCN as eluents. Fractions containing the desired compound were lyophilized to dryness to afford *N*-benzyl-4-(2-cyanophenoxy)benzamide (54 mg, 40%) as a white solid. ^{1}H NMR (400.13 MHz, DMSO-d_6) δ 4.50 (2H, d, J = 5.6 Hz), 7.11−7.13 (1H, m), 7.19−7.22 (2H, m), 7.24−7.27 (1H, m), 7.32−7.39 (5H, m), 7.70−7.75

dx.doi.org/10.1021/jm501038s | J. Med. Chem. XXXX, XXX, XXX−XXX

(1H, m), 7.94 (1H, dd, J = 8.1 Hz, J = 2.0 Hz), 7.98–8.02 (2H, m), 9.04 (1H, t, J = 5.6 Hz); ESI$^-$ m/z $(M - H)^-$ 327.66.

*4-(2-Cyanophenoxy)-N-(pyridin-3-ylmethyl)benzamide (**10**).*

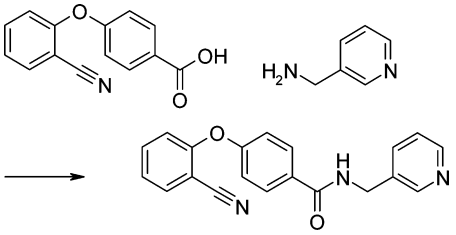

A solution of 4-(2-cyanophenoxy)benzoic acid (100 mg, 0.42 mmol) and HATU (160 mg, 0.42 mmol) was allowed to stir at room temperature for 5 min before adding 3-aminomethylpyridine (43 mg, 0.40 mmol) and DIPEA (350 μL, 2.0 mmol). This solution was allowed to stir at room temperature overnight. The reaction mixture was diluted with acetonitrile (1 mL), water (2 mL) and ammonium hydroxide (0.5 mL) before purifying by reverse phase base (NH_4OH) modified preparative HPLC. Pure fractions were combined and evaporated before being lyophilized (freeze-dried) overnight. There was thus obtained 4-(2-cyanophenoxy)-*N*-(pyridin-3-ylmethyl)benzamide (108 mg, 77%) as a white solid. ^{1}H NMR (400.13 MHz, DMSO-d_6) δ 4.51 (2H, d, J = 5.8 Hz), 7.12 (1H, d, J = 8.8 Hz), 7.20–7.23 (2H, m), 7.35–7.39 (2H, m), 7.70–7.75 (2H, m), 7.94–8.01 (3H, m), 8.46–8.48 (1H, m), 8.56 (1H, d, J = 2.0 Hz), 9.14 (1H, t, J = 5.8 Hz); ^{13}C NMR (176 MHz, DMSO-d_6, 30 °C) 40.38, 103.56, 115.57, 118.38, 118.80, 123.35, 124.53, 129.63, 130.28, 134.20, 134.96, 135.01, 135.36, 147.99, 148.75, 157.61, 157.67, 165.36; ESI$^+$ m/z $(M + H)^+$ 330.32; ESI-HRMS calculated for $C_{20}H_{15}N_3O_2$ $(M + H)^+$ 330.1243; found, 330.1267.

*4-(2-Cyanophenoxy)-N-(pyrimidin-4-ylmethyl)benzamide (**11**).*

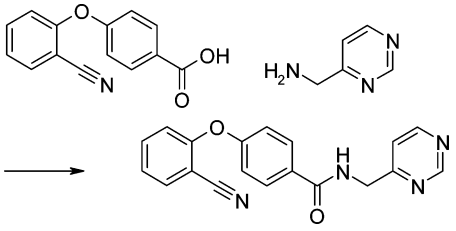

A solution of 4-(2-cyanophenoxy)benzoic acid (100 mg, 0.42 mmol) and HATU (160 mg, 0.42 mmol) was allowed to stir at room temperature for 5 min before addition of 4-aminomethylpyrimidine (43 mg, 0.40 mmol) and DIPEA (350 μL, 2.0 mmol). This solution was allowed to stir at room temperature overnight. The reaction mixture was diluted with acetonitrile (1 mL), water (2 mL), and ammonium hydroxide (0.5 mL) before purifying by reverse phase base (NH_4OH) modified preparative HPLC. Pure fractions were combined and evaporated before being lyophilized (freeze-dried) overnight. 4-(2-Cyanophenoxy)-*N*-(pyrimidin-4-ylmethyl)benzamide (102 mg, 77%) was thus obtained as a white solid. ^{1}H NMR (400.13 MHz, DMSO-d_6) δ 4.56 (2H, d, J = 5.8 Hz), 7.14 (1H, d, J = 8.2 Hz), 7.22–7.26 (2H, m), 7.36–7.40 (1H, m), 7.44–7.46 (1H, m), 7.72–7.76 (1H, m), 7.95–7.97 (1H, m), 8.01–8.04 (2H, m), 8.74 (1H, d, J = 6.0 Hz), 9.12 (1H, s), 9.24 (1H, t, J = 5.8 Hz); ESI$^+$ m/z $(M + H)^+$ 331.

*N-[5-(Dimethylsulfamoyl)-2-methylphenyl]-1-phenyl-5-propyl-1H-pyrazole-4-carboxamide (**12**).*

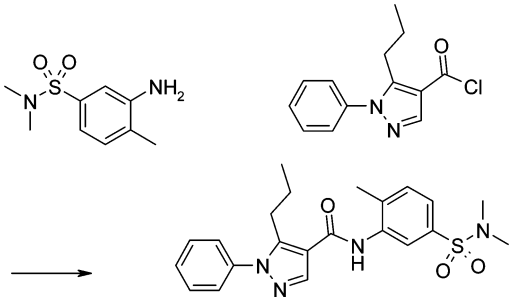

3-Amino-*N*,*N*-4-trimethylbenzenesulfonamide (152 mg, 0.71 mmol) was added in one portion to 1-phenyl-5-propyl-1*H*-pyrazole-4-carbonyl chloride (176 mg, 0.71 mmol) in THF (4 mL) at 20 °C under air. The resulting suspension was stirred at 20 °C for 16 h. The solvents were then removed *in vacuo* to give a yellow solid. The crude product was purified by preparative HPLC (Waters XBridge Prep C18 OBD column, 5 μm silica, 21 mm diameter, 150 mm length), using decreasingly polar mixtures of water (containing 0.1% formic acid) and MeCN as eluents. Fractions containing the desired compound were evaporated to dryness to afford *N*-[5-(dimethylsulfamoyl)-2-methylphenyl]-1-phenyl-5-propyl-1*H*-pyrazole-4-carboxamide (172 mg, 57%) as a white solid. ^{1}H NMR (400.13 MHz, DMSO-d_6) δ 0.76 (3H, t, J = 7.8 Hz), 1.40–1.51 (2H, m), 2.38 (3H, s), 2.66 (6H, s), 2.97 (2H, t, J = 7.2 Hz), 7.49–7.64 (7H, m), 7.79 (1H, s), 8.32 (1H, s) and 9.70 (1H, s); ^{13}C NMR (176 MHz, DMSO-d_6, 30 °C) 13.49, 18.04, 21.67, 25.97, 37.52, 114.58, 124.24, 124.66, 125.82, 128.77, 129.29, 131.17, 132.30, 137.01, 138.70, 138.79, 139.38, 146.53, 161.47; ESI$^+$ m/z $(M + H)^+$ 427.24; ESI-HRMS calculated for $C_{22}H_{26}N_4O_3S$ $(M + H^+)$ 427.17984; found, 427.17978.

*N-(5-Fluoro-2-methylphenyl)-1-phenyl-5-propyl-1H-pyrazole-4-carboxamide (**13**).*

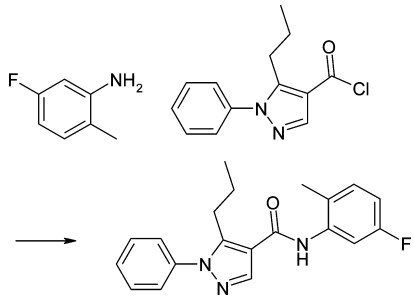

2-Amino-4-fluorotoluene (252 mg, 2.0 mmol) was added in one portion to 1-phenyl-5-propyl-1*H*-pyrazole-4-carbonyl chloride (500 mg, 2.0 mmol) in THF (8 mL) at 20 °C under air. The resulting suspension was stirred at 20 °C for 16 h. The solvents were then removed *in vacuo* to give a yellow solid. This was then dissolved in DMSO/acetonitrile/water and basified with concentrated ammonia solution. The solid that was precipitated was filtered off, washed with acetonitrile and water, and then dried overnight under high vacuum to give *N*-(5-fluoro-2-methylphenyl)-1-phenyl-5-propyl-1*H*-pyrazole-4-carboxamide (358 mg, 53%) as a white solid. ^{1}H NMR (400.13 MHz, DMSO-d_6) δ 0.75 (3H, t, J = 7.6 Hz), 1.40–1.51 (2H, m), 2.26 (3H, s), 2.96 (2H, t, J = 8.2 Hz), 6.96–7.02 (1H, ddd, J = 8.0 Hz, J = 7.8 Hz, J = 2.8 Hz), 7.27–7.33 (2H, m), 7.48–7.52 (5H, m), 8.29 (1H, s) and 8.99 (1H, s); ESI$^+$ m/z $(M + H)^+$ 338.18.

*N-(5-Cyano-2-methylphenyl)-1-phenyl-5-propyl-1H-pyrazole-4-carboxamide (**14**).*

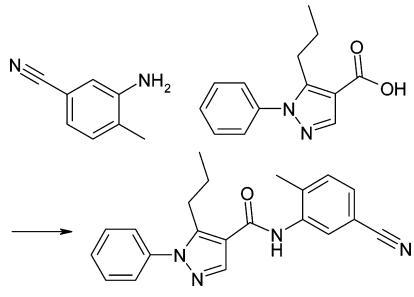

HATU (410 mg, 1.08 mmol) was added to a solution of 1-phenyl-5-propyl-1*H*-pyrazole-4-carboxylic acid (207 mg, 0.90 mmol) in DMF (2 mL), and the reaction mixture was stirred at ambient temperature for 10 min. 3-Amino-4-methylbenzonitrile (119 mg, 0.90 mmol) and DIPEA (0.47 mL, 2.7 mmol) were then added, and the reaction mixture was stirred for a further 2 h, then diluted to 10 mL with acetonitrile and left to stand for 5 days, during which time a precipitate formed. This was filtered, washed with water (3 × 10 mL), and dried under vacuum to give *N*-(5-cyano-2-methylphenyl)-1-phenyl-5-propyl-1*H*-pyrazole-4-carboxamide (47 mg, 15%) as a white solid. ^{1}H NMR (400.13 MHz, DMSO-d_6) δ 0.74 (3H, t, J = 7.6 Hz), 1.37–1.5 (2H, m), 2.35 (3H, s),

dx.doi.org/10.1021/jm501038s | J. Med. Chem. XXXX, XXX, XXX–XXX

2.88−2.97 (2H, m), 7.47−7.65 (7H, m), 7.85 (1H, d, J = 2.2 Hz), 8.32 (1H, s), 9.71 (1H, s); ESI$^+$ m/z $(M + H)^+$ 345.52.

*N-(5-Hydroxy-2-methylphenyl)-1-phenyl-5-propyl-1H-pyrazole-4-carboxamide (**15**).*

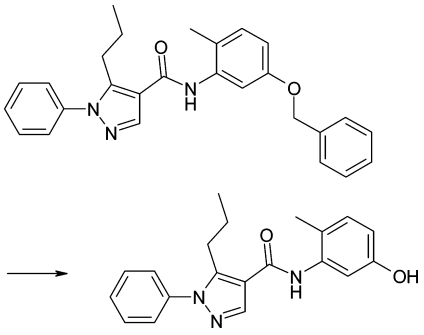

N-(5-(Benzyloxy)-2-methylphenyl)-1-phenyl-5-propyl-1*H*-pyrazole-4-carboxamide (150 mg, 0.35 mmol) and palladium on carbon (37.5 mg, 0.35 mmol) in ethanol (10 mL) was stirred under an atmosphere of hydrogen at 5 bar and 40 °C for 16 h. The catalyst was then filtered off through Celite, and the filtrate was concentrated *in vacuo* to give a yellow solid. The crude product was purified by preparative HPLC (Phenomenex Gemini C18 110A (axia) column, 5 μm silica, 21 mm diameter, 100 mm length), using decreasingly polar mixtures of water (containing 0.1% formic acid) and MeCN as eluents. Fractions containing the desired compound were evaporated to dryness to afford *N*-(5-hydroxy-2-methylphenyl)-1-phenyl-5-propyl-1*H*-pyrazole-4-carboxamide (72 mg, 61%) as a white solid. ^{1}H NMR (400.13 MHz, DMSO-d_6) δ 0.66 (3H, t, J = 7.8 Hz), 1.30−1.40 (2H, m), 2.05 (3H, s), 2.85 (2H, t, J = 8.4 Hz), 6.48 (1H, dd, J = 8.4 Hz, J = 2.6 Hz), 6.75 (1H, d, J = 2.6 Hz), 6.94 (1H, d, J = 8.4 Hz), 7.40−7.54 (5H, m), 8.18 (1H, s), 9.15 (1H, s) and 9.28 (1H, s); ESI$^+$ m/z $(M + H)^+$ 336.25.

*N-(5-Benzyloxy-2-methyl-phenyl)-1-phenyl-5-propyl-1H-pyrazole-4-carboxamide (**16**).*

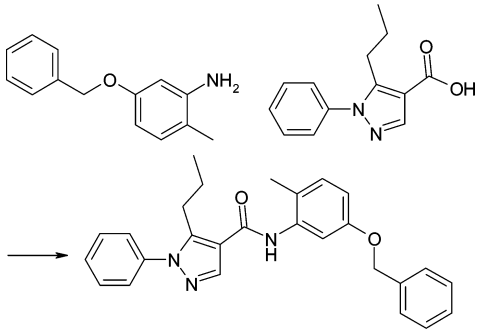

A solution of HATU (226 mg, 0.59 mmol) in DMF (1 mL) was added to 1-phenyl-5-propyl-1*H*-pyrazole-4-carboxylic acid (114 mg, 0.50 mmol), and the reaction mixture was stirred for 10 min. A solution of 5-benzyloxy-2-methyl-aniline (105 mg, 0.50 mmol) and DIPEA (260 μL, 1.5 mmol) in DMF (1 mL) was then added, and the reaction mixture was stirred at ambient temperature for 16 h, then diluted to 5 mL with acetonitrile/water and purified by reverse-phase prep-HPLC, eluting with a gradient of acetonitrile/water (0.1% NH_3). Product fractions were combined and evaporated under reduced pressure to give *N*-(5-benzyloxy-2-methyl-phenyl)-1-phenyl-5-propyl-1*H*-pyrazole-4-carboxamide as a white solid (169 mg, 79%). ^{1}H NMR (700 MHz, DMSO-d_6) δ 0.74 (3H, t, J = 7.4 Hz), 1.42−1.48 (2H, m), 2.18 (3H, s), 2.95 (2H, t, J = 6.7 Hz), 5.10 (2H, s), 6.84 (1H, dd, J = 7.7 Hz, J = 2.0 Hz), 7.06 (1H, d, J = 2.0 Hz), 7.17 (1H, d, J = 8.4 Hz), 7.34 (1H, m), 7.38−7.42 (2H, m), 7.45−7.48 (2H, m), 7.48−7.51 (2H, m), 7.52−7.56 (1H, m), 7.57−7.61 (2H, m), 8.28 (1H, s), 9.43 (1H, s); ESI$^-$ m/z $(M - H)^-$ 425.

*Methyl 4-Methyl-3-(1-phenyl-5-propyl-1H-pyrazole-4-carboxamido)benzoate (**17**).*

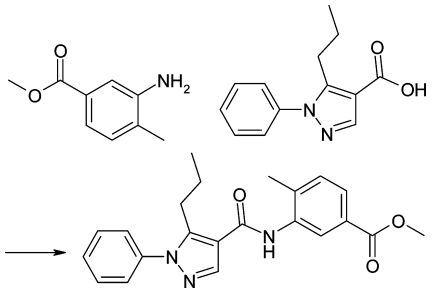

A solution of HATU (226 mg, 0.59 mmol) in DMF (1 mL) was added to 1-phenyl-5-propyl-1*H*-pyrazole-4-carboxylic acid (114 mg, 0.50 mmol), and the reaction mixture was stirred for 10 min. A solution of methyl 3-amino-4-methylbenzoate (83 mg, 0.50 mmol) and DIPEA (260 μL, 1.5 mmol) in DMF (1 mL) was then added, and the reaction mixture was stirred at ambient temperature for 16 h, then diluted to 5 mL with acetonitrile/water and purified by reverse-phase prep-HPLC, eluting with a gradient of acetonitrile/water (0.1% ammonia). Product fractions were combined and evaporated under reduced pressure to give methyl 4-methyl-3-(1-phenyl-5-propyl-1*H*-pyrazole-4-carboxamido)benzoate (105 mg, 56%) as a white solid. ^{1}H NMR (700 MHz, DMSO-d_6) δ 0.75 (3H, t, J = 7.8 Hz), 1.45 (2H, m), 2.34 (3H, s), 2.92−2.98 (2H, m), 3.87 (3H, s), 7.44 (1H, d, J = 7.4 Hz), 7.51 (2H, m), 7.53−7.57 (1H, m), 7.58−7.62 (2H, m), 7.76 (1H, dd, J = 8.0 Hz, J = 2.1 Hz), 7.99 (1H, d, J = 2.1 Hz), 8.31 (1H, s), 9.63 (1H, s); ESI$^-$ m/z $(M - H)^-$ 377.

*N-(2-Methyl-5-methylsulfonyl-phenyl)-1-phenyl-5-propyl-1H-pyrazole-4-carboxamide (**18**).*

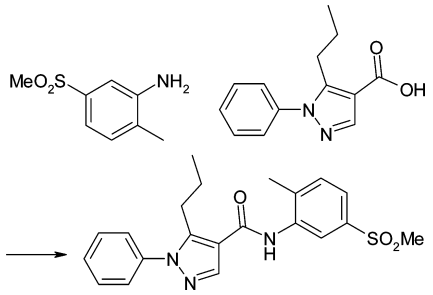

A solution of HATU (226 mg, 0.59 mmol) in DMF (1 mL) was added to 1-phenyl-5-propyl-1*H*-pyrazole-4-carboxylic acid (114 mg, 0.50 mmol), and the reaction mixture was stirred for 10 min. A solution of 2-methyl-5-methylsulfonyl-aniline (92 mg, 0.50 mmol) and DIPEA (260 μL, 1.5 mmol) in DMF (1 mL) was then added, and the reaction mixture was stirred at ambient temperature for 16 h, then diluted to 5 mL with acetonitrile/water and purified by reverse-phase prep-HPLC, eluting with a gradient of acetonitrile/water (0.1% NH_3). Product fractions were combined and evaporated under reduced pressure to give *N*-(2-methyl-5-methylsulfonyl-phenyl)-1-phenyl-5-propyl-1*H*-pyrazole-4-carboxamide as a white solid (36 mg, 18%). ^{1}H NMR (700 MHz, DMSO-d_6) δ 0.74 (3H, t, J = 7.4 Hz), 1.41−1.48 (2H, m), 2.37 (3H, s), 2.92−2.97 (2H, m), 7.49−7.51 (2H, m), 7.53−7.57 (2H, m), 7.59 (2H, m), 7.70 (1H, dd, J = 8.8 Hz, J = 2.6 Hz), 7.96 (1H, d, J = 2.5 Hz), 8.31 (1H, s), 9.72 (1H, s); ESI$^-$ m/z $(M - H)^-$ 397.

*4-Methyl-3-(1-phenyl-5-propyl-1H-pyrazole-4-carboxamido)-benzoic acid (**19**).*

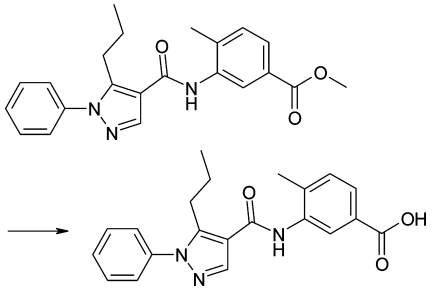

dx.doi.org/10.1021/jm501038s | J. Med. Chem. XXXX, XXX, XXX−XXX

Methyl 4-methyl-3-(1-phenyl-5-propyl-1*H*-pyrazole-4-carboxamido)-benzoate (82 mg, 0.22 mmol) was dissolved in tetrahydrofuran (1 mL). Aqueous sodium hydroxide (2 M, 1.1 mL, 2.2 mmol) was added, followed by methanol (0.5 mL), and the reaction mixture was stirred at ambient temperature for 16 h. The reaction mixture was then evaporated at reduced pressure, redissolved in water (5 mL), and acidified to pH 1 with 2 M aqueous HCl. The resulting precipitate was filtered, washed with water (2 × 5 mL), and dried under vacuum to give 4-methyl-3-(1-phenyl-5-propyl-1*H*-pyrazole-4-carboxamido)benzoic acid (66 mg, 84%) as a white solid. ^{1}H NMR (400.13 MHz, DMSO-d_6) δ 0.80 (3H, t, J = 7.6 Hz), 1.50 (2H, m), 2.40 (3H, s), 3.00 (2H, m), 7.45 (1H, d, J = 8.3 Hz), 7.60 (5H, m), 7.80 (1H, dd, J = 8.3 Hz, J = 2.0 Hz), 8.00 (1H, m), 8.37 (1H, s), 9.72 (1H, s), 12.95 (1H, s); ESI$^-$ m/z (M − H)$^-$ 362.26.

*1-(4-Chlorophenyl)-N-(5-(N,N-dimethylsulfamoyl)-2-methylphenyl)-5-propyl-1H-pyrazole-4-carboxamide (**20**).*

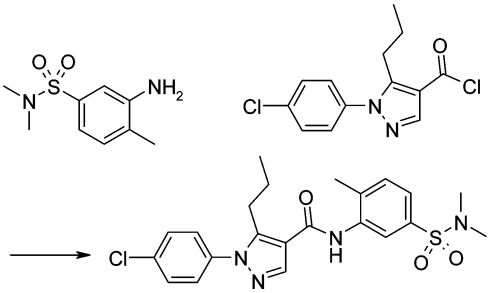

3-Amino-4,*N*,*N*-trimethyl-benzenesulfonamide (55 mg, 0.26 mmol) was added in one portion to 1-(4-chlorophenyl)-5-propyl-1*H*-pyrazole-4-carbonyl chloride (73 mg, 0.26 mmol) in THF (2 mL) at 20 °C under nitrogen. The resulting suspension was stirred at 20 °C for 16 h. The solvents were removed *in vacuo*. The residue was then dissolved in DCM (20 mL) and washed with saturated sodium bicarbonate solution (20 mL). The DCM layer was passed through a phase separating cartridge and concentrated under reduced pressure to give crude product. The crude product was purified by preparative HPLC (Phenomenex Gemini C18 110A (axia) column, 5 μm silica, 21 mm diameter, 100 mm length), using decreasingly polar mixtures of water (containing 0.1% formic acid) and MeCN as eluents. Fractions containing the desired compound were evaporated to dryness to afford 1-(4-chlorophenyl)-*N*-(5-(*N*,*N*-dimethylsulfamoyl)-2-methylphenyl)-5-propyl-1*H*-pyrazole-4-carboxamide (58 mg, 49%) as a white solid. ^{1}H NMR (400.13 MHz, $CDCl_3$) δ 0.86 (3H, t, J = 7.6 Hz), 1.53−1.63 (2H, m), 2.42 (3H, s), 2.76 (6H, s), 2.99 (2H, t, J = 8.0 Hz), 7.35−7.42 (3H, m), 7.46 (1H, s), 7.49−7.53 (3H, m), 7.94 (1H, s) and 8.29 (1H, s); ESI$^-$ m/z (M − H)$^-$ 459.10.

*N-(5-(N,N-Dimethylsulfamoyl)-2-methylphenyl)-5-propyl-1-(pyridin-3-yl)-1H-pyrazole-4-carboxamide (**21**).*

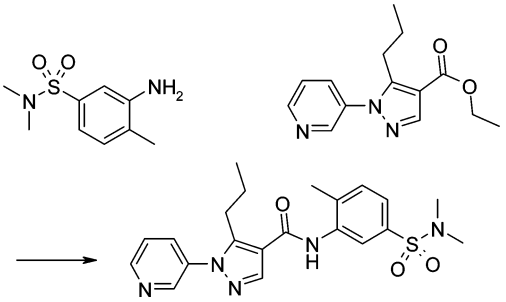

Trimethylaluminum (1.5 mL, 3.0 mmol) was added dropwise to ethyl 5-propyl-1-(pyridin-3-yl)-1*H*-pyrazole-4-carboxylate (192 mg, 0.74 mmol) and 3-amino-4,*N*,*N*-trimethyl-benzenesulfonamide (317 mg, 1.48 mmol) in DCM (5 mL) at 20 °C under nitrogen. The resulting solution was stirred at 20 °C for 16 h. The reaction was quenched by careful addition of a saturated solution of Rochelle's salt (10 mL). The reaction mixture was extracted twice with DCM (2 × 15 mL), the combined organics were passed through a phase separating cartridge and concentrated under reduced pressure to give a yellow gum. The crude product was purified by preparative HPLC (Phenomenex Gemini C18 110A (axia) column, 5 μm silica, 21 mm diameter, 100 mm length), using decreasingly polar mixtures of water (containing 0.1% formic acid) and MeCN as eluents. Fractions containing the desired compound were evaporated to dryness to afford *N*-(5-(*N*,*N*-dimethylsulfamoyl)-2-methylphenyl)-5-propyl-1-(pyridin-3-yl)-1*H*-pyrazole-4-carboxamide (130 mg, 41%) as a white solid. ^{1}H NMR (400.13 MHz, DMSO-d_6) δ 0.67 (3H, t, J = 7.6 Hz), 1.29−1.39 (2H, m), 2.27 (3H, s), 2.55 (6H, s), 2.88 (2H, t, J = 8.2 Hz), 7.43−7.50 (2H, m), 7.57 (1H, dd, J = 8.0 Hz, J = 5.0 Hz), 7.69 (1H, s), 7.95 (1H, d, J = 8.0 Hz), 8.31 (1H, s), 8.64−8.72 (2H, m), 9.74 (1H, s); ESI$^+$ m/z (M + H)$^+$ 428.31.

*Ethyl 5-propyl-1-(pyridin-3-yl)-1H-pyrazole-4-carboxylate (**28a**).*

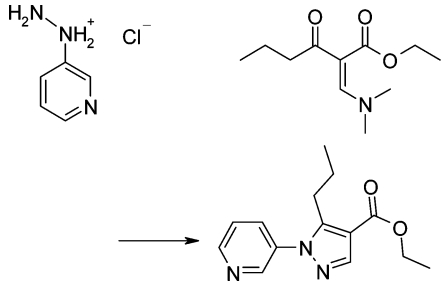

1-(Pyridin-3-yl)hydrazinium chloride (3.50 g, 24.0 mmol) was added in one portion to (*Z*)-ethyl 2-((dimethylamino)methylene)-3-oxohexanoate (5.13 g, 24.0 mmol) in ethanol (70 mL) at 20 °C under air. The resulting solution was stirred at 80 °C for 16 h. The reaction mixture was then concentrated *in vacuo* to give an orange oil. This was then dissolved in ethyl acetate (100 mL) and washed with saturated sodium bicarbonate solution (100 mL), the layers were separated, the aqueous layer was re-extracted with ethyl acetate (100 mL), and the combined organic layers were washed with brine (100 mL), dried (Na_2SO_4), filtered, and evaporated to give an orange oil. The crude product was purified by flash silica chromatography, elution gradient 0−50% EtOAc in isohexane. Pure fractions were evaporated to dryness to afford ethyl 5-propyl-1-(pyridin-3-yl)-1*H*-pyrazole-4-carboxylate (4.84 g, 78%) as a yellow gum. ^{1}H NMR (400.13 MHz, $CDCl_3$) δ 0.90 (3H, t), 1.39 (3H, t), 1.55−1.67 (2H, m), 2.94 (2H, t), 4.33 (2H, q), 7.47−7.52 (1H, m), 7.78−7.82 (1H, m), 8.08 (1H, s) and 8.70−8.74 (2H, m); ESI$^+$ m/z (M + H)$^+$ 260.50.

*1-Benzyl-N-(5-(N,N-dimethylsulfamoyl)-2-methylphenyl)-5-propyl-1H-pyrazole-4-carboxamide (**22**).*

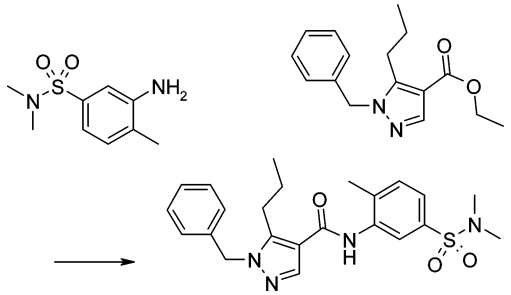

Trimethylaluminum (1.63 mL, 3.26 mmol) was added dropwise to ethyl 1-benzyl-5-propyl-1*H*-pyrazole-4-carboxylate (222 mg, 0.82 mmol) and 3-amino-4,*N*,*N*-trimethyl-benzenesulfonamide (349 mg, 1.63 mmol) in DCM (5 mL) at 20 °C under nitrogen. The resulting solution was stirred at 20 °C for 16 h. The reaction was quenched by careful addition of a saturated solution of Rochelle's salt (10 mL). The reaction mixture was extracted twice with DCM (2 × 15 mL), and the combined organic layers were passed through a phase separating cartridge and concentrated under reduced pressure to give a yellow gum. The crude product was purified by preparative HPLC (Phenomenex Gemini C18 110A (axia) column, 5 μm silica, 21 mm diameter, 100 mm length), using decreasingly polar mixtures of water (containing 0.1% formic acid) and MeCN as eluents. Fractions containing the desired compound were evaporated to dryness to afford 1-benzyl-*N*-(5-(*N*,*N*-dimethylsulfamoyl)-2-methylphenyl)-5-propyl-1*H*-pyrazole-4-carboxamide (288 mg, 80%) as a white solid. ^{1}H NMR (400.13 MHz, DMSO-d_6) δ 0.83 (3H, t, J = 7.6 Hz), 1.35−1.45 (2H, m), 2.35 (3H, s), 2.61 (6H, s), 2.94 (2H, t, J = 8.4 Hz),

dx.doi.org/10.1021/jm501038s | J. Med. Chem. XXXX, XXX, XXX−XXX

5.40 (2H, s), 7.19 (2H, d, J = 7.2 Hz), 7.28–7.40 (3H, m), 7.48–7.55 (2H, m), 7.77 (1H, s), 8.18 (1H, s) and 9.59 (1H, s); ESI$^-$ m/z (M − H)$^-$ 439.23.

*Ethyl 1-Benzyl-5-propyl-1H-pyrazole-4-carboxylate (**28b**).*

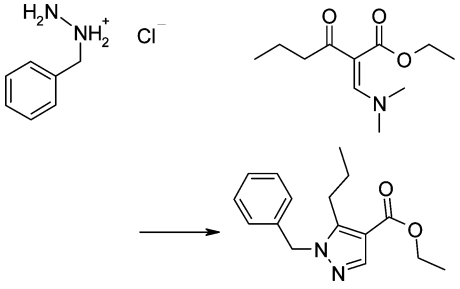

Benzylhydrazine dihydrochloride (3.98 g, 20.4 mmol) was added to (*Z*)-ethyl 2-((dimethylamino)methylene)-3-oxohexanoate (2.90 g, 13.6 mmol) and acetic acid (0.078 mL, 1.36 mmol) in ethanol (160 mL) at 20 °C under air. The resulting solution was stirred at 80 °C for 16 h and then concentrated *in vacuo* yielding a yellow oil. This was diluted with EtOAc (600 mL) and washed with sodium bicarbonate (200 mL), followed by water (200 mL) and brine (200 mL). The organic layer was dried using $MgSO_4$, filtered, and evaporated to afford the crude product. The crude product was purified by flash silica chromatography, elution gradient 0 to 15% EtOAc in isohexane. Pure fractions were evaporated to dryness to afford ethyl 1-benzyl-5-propyl-1*H*-pyrazole-4-carboxylate (2.89 g, 78%) as a yellow oil. ^{1}H NMR (400.13 MHz, $CDCl_3$) δ 0.92 (3H, t), 1.33–1.36 (3H, t), 1.44–1.54 (2H, m), 2.86–2.90 (2H, m), 4.28 (2H, q), 5.32 (2H, s), 7.10 (2H, d), 7.25–7.34 (3H, m), 7.92 (1H, s); ESI$^+$ m/z (M + H)$^+$ 273.51.

*N-(5-(N,N-Dimethylsulfamoyl)-2-methylphenyl)-1-isobutyl-5-propyl-1H-pyrazole-4-carboxamide (**23**).*

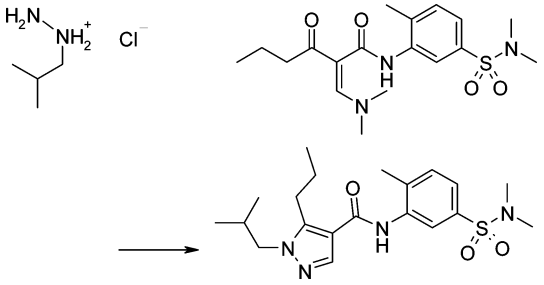

Isobutylhydrazine hydrochloride (62 mg, 0.50 mmol) was added to 2-((dimethylamino)methylene)-*N*-(5-(*N*,*N*-dimethylsulfamoyl)-2-methylphenyl)-3-oxohexanamide (126 mg, 0.33 mmol) and acetic acid (1.89 μL, 0.03 mmol) in ethanol (10 mL) at 20 °C under air. The resulting solution was stirred at 80 °C for 1.25 h, then cooled and evaporated to give a yellow oil. The crude product was purified by preparative HPLC Waters XBridge Prep C18 OBD column, 5 μm silica, 19 mm diameter, 100 mm length, using decreasingly polar mixtures of water (containing 0.1% NH_3) and MeCN as eluents. Fractions containing the desired compound were lyophilized to dryness to afford *N*-(5-(*N*,*N*-dimethylsulfamoyl)-2-methylphenyl)-1-isobutyl-5-propyl-1*H*-pyrazole-4-carboxamide (34 mg, 25%) as a pale yellow solid. ^{1}H NMR (400.13 MHz, DMSO-d_6) δ 0.87 (3H, s), 0.89 (3H, s), 0.91 (3H, t, J = 7.4 Hz), 1.50–1.60 (2H, m), 2.16–2.22 (1H, m), 2.33 (3H, s), 2.62 (6H, s), 2.95 (2H, t, J = 7.8 Hz), 3.90 (2H, d, J = 7.6 Hz), 7.48–7.54 (2H, m), 7.75–7.77 (1H, m), 8.10 (1H, s), 9.55 (1H, s); ESI$^+$ m/z (M + H)$^+$ 407.

*2-((Dimethylamino)methylene)-N-(5-(N,N-dimethylsulfamoyl)-2-methylphenyl)-3-oxohexanamide (**31**).*

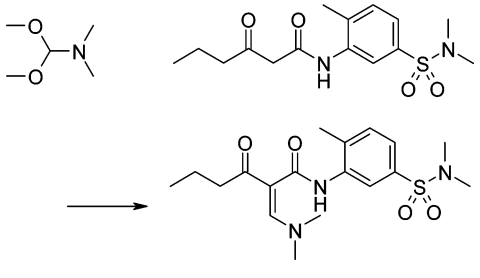

1,1-Dimethoxy-*N*,*N*-dimethylmethanamine (0.445 mL, 3.32 mmol) was added to *N*-(5-(*N*,*N*-dimethylsulfamoyl)-2-methylphenyl)-3-oxohexanamide (868 mg, 2.66 mmol) in dioxane (10 mL), and the resulting solution was stirred at 100 °C for 1 h. The resulting mixture was cooled and evaporated to dryness to afford 2-((dimethylamino)methylene)-*N*-(5-(*N*,*N*-dimethylsulfamoyl)-2-methylphenyl)-3-oxohexanamide (1.17 g, quant.) as a brown oil, which solidified on standing. ^{1}H NMR (400.13 MHz, DMSO-d_6) δ 0.92 (3H, s), 1.56–1.65 (2H, m), 2.39 (3H, s), 2.54 (2H, t), 2.60–2.66 (6H, s), 3.15 (6H, s), 7.32–7.35 (1H, m), 7.42 (1H, d), 7.81 (1H, s), 8.37 (1H, s); ESI$^-$ m/z (M − H)$^-$ 380.

*N-(5-(N,N-Dimethylsulfamoyl)-2-methylphenyl)-3-oxohexanamide (**30**).*

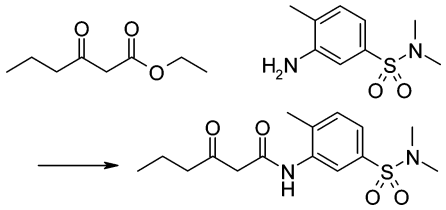

3-Amino-*N*,*N*-4-trimethylbenzenesulfonamide (1.84 g, 8.59 mmol) and ethyl 3-oxohexanoate (1.36 mL, 8.59 mmol) were dissolved in acetic acid (10 mL) and sealed into a microwave tube. The reaction was heated to 150 °C for 30 min in the microwave reactor and cooled to RT. The reaction mixture was evaporated, then neutralized with saturated $NaHCO_3$ and extracted with Et_2O. The crude product was purified by flash silica chromatography, elution gradient 10–50% EtOAc in isohexane. Pure fractions were evaporated to dryness to afford *N*-(5-(*N*,*N*-dimethylsulfamoyl)-2-methylphenyl)-3-oxohexanamide (0.87 g, 31%) as a yellow gum. ^{1}H NMR (400.13 MHz, DMSO-d_6) δ 0.88 (3H, s), 1.48–1.57 (2H, m), 2.33 (3H, s), 2.53–2.58 (2H, m), 2.60 (6H, s), 3.63 (2H, d), 7.43–7.45 (1H, m), 7.50 (1H, d), 7.94 (1H, d), 9.69 (1H, s); ESI$^+$ m/z (M + H)$^+$ 327.

■ ASSOCIATED CONTENT

Supporting Information

Data collection and refinement statistics for X-ray crystal structures, Biacore data for compounds **6** and **12**, ^{1}H NMR spectra for compounds **6**–**23**, and details of biochemical results for compounds **2**–**23**. This material is available free of charge via the Internet at http://pubs.acs.org.

■ AUTHOR INFORMATION

Corresponding Author

*Phone: +41 (0) 61 687 11 71. E-mail: john_g.cumming@roche.com.

Notes

The authors declare no competing financial interest.

■ ACKNOWLEDGMENTS

The authors thank our colleagues Brian Ellershaw, Robert Forder, and Christine Harding for developing and carrying out the biological assays. Pernilla Löfås, Ewa Nilsson, David Hargreaves, and Michael Mrosek are thanked for protein preparation and crystallization for structural studies, and Marie Fraser is thanked for some of the structure refinement. We also thank Andrew Stanier for synthesis support and Andrew Pape for chemistry design input.

■ ABBREVIATIONS USED

DIPEA, *N*,*N*-diisopropylethylamine; DMEM, Dulbecco/Vogt modified Eagle's minimal essential medium; FCS, fetal calf serum; HATU, 1-[bis(dimethylamino)methylene]-1*H*-1,2,3-triazolo[4,5-*b*]pyridinium 3-oxide hexafluorophosphate; HEPES, 4-(2-hydroxyethyl)-1-piperazineethanesulfonic acid; HRP, horseradish peroxidase; hPBMC, human peripheral

dx.doi.org/10.1021/jm501038s | J. Med. Chem. XXXX, XXX, XXX–XXX

blood mononuclear cell; IL-1, interleukin-1; IoC, inhibition of catalysis; ISA, inhibition in solution assay; LPS, lipopolysaccharide; MBP, myelin basic protein; MES, 2-(*N*-morpholino)-ethanesulfonic acid; MOPS, 3-(*N*-morpholino)propanesulfonic acid; PGE_2, prostaglandin E2; PoA, prevention of activation; SEM, standard error of the mean; TBST, tris-buffered saline with tween; TCEP, tris(2-carboxyethyl)phosphine; TDC, target definition compound; TROSY-HSQC, transverse relaxation optimized spectroscopy with heteronuclear single quantum coherence

REFERENCES

(1) Kumar, S.; Boehm, J.; Lee, J. C. p38 MAP kinases: Key signalling molecules as therapeutic targets for inflammatory diseases. *Nat. Rev. Drug Discovery* **2003**, *2*, 717−726.

(2) Schieven, G. L. The biology of p38 kinase: A central role in inflammation. *Curr. Top. Med. Chem.* **2005**, *5*, 921−928.

(3) Schieven, G. L. The p38alpha kinase plays a central role in inflammation. *Curr. Top. Med. Chem.* **2009**, *9*, 1038−1048.

(4) Weaver, A. L. The impact of new biologicals in the treatment of rheumatoid arthritis. *Rheumatology (Oxford)* **2004**, *43* (Suppl 3), iii17−iii23.

(5) Scheinecker, C.; Smolen, J.; Yasothan, U.; Stoll, J.; Kirkpatrick, P. Tocilizumab. *Nat. Rev. Drug Discovery* **2009**, *8*, 273−274.

(6) Fischer, S.; Koeberle, S. C.; Laufer, S. A. P38alpha Mitogen-Activated Protein Kinase Inhibitors, a Patent Review (2005−2011). *Expert Opin. Ther. Pat.* **2011**, *21*, 1843−1866.

(7) Amir, M.; Somakala, K.; Ali, S. P38 MAP Kinase Inhibitors as Anti inflammatory Agents. *Mini-Rev. Med. Chem.* **2013**, *13*, 2082−2096.

(8) Sweeney, S. E. The as-yet unfulfilled promise of p38 MAPK inhibitors. *Nat. Rev. Rheumatol.* **2009**, *5*, 475−477.

(9) Goldstein, D. M.; Kuglstatter, A.; Lou, Y.; Soth, M. J. Selective p38α Inhibitors Clinically Evaluated for the Treatment of Chronic Inflammatory Disorders. *J. Med. Chem.* **2010**, *53*, 2345−2353.

(10) Aston, N. M.; Bamborough, P.; Buckton, J. B.; Edwards, C. D.; Holmes, D. S.; Jones, K. L.; Patel, V. K.; Smee, P. A.; Somers, D. O.; Vitulli, G.; Walker, A. L. p38α Mitogen-Activated Protein Kinase Inhibitors: Optimization of a Series of Biphenylamides to Give a Molecule Suitable for Clinical Progression. *J. Med. Chem.* **2009**, *52*, 6257−6269.

(11) Zhang, J.; Shen, B.; Lin, A. Novel strategies for inhibition of the p38 MAPK pathway. *Trends Pharmacol. Sci.* **2007**, *28*, 286−295.

(12) Davidson, W.; Frego, L.; Peet, G. W.; Kroe, R. R.; Labadia, M. E.; Lukas, S. M.; Snow, R. J.; Jakes, S.; Grygon, C. A.; Pargellis, C.; Werneburg, B. G. Discovery and characterization of a substrate selective p38alpha inhibitor. *Biochemistry* **2004**, *43*, 11658−11671.

(13) Winzen, R.; Kracht, M.; Ritter, B.; Wilhelm, A.; Chen, C. Y.; Shyu, A. B.; Muller, M.; Gaestel, M.; Resch, K.; Holtmann, H. The p38 MAP kinase pathway signals for cytokine-induced mRNA stabilization via MAP kinase-activated protein kinase 2 and an AU-rich region-targeted mechanism. *EMBO J.* **1999**, *18*, 4969−4980.

(14) Neininger, A.; Kontoyiannis, D.; Kotlyarov, A.; Winzen, R.; Eckert, R.; Volk, H. D.; Holtmann, H.; Kollias, G.; Gaestel, M. MK2 targets AU-rich elements and regulates biosynthesis of tumor necrosis factor and interleukin-6 independently at different post-transcriptional levels. *J. Biol. Chem.* **2002**, *277*, 3065−3068.

(15) Hegen, M.; Gaestel, M.; Nickerson-Nutter, C. L.; Lin, L. L.; Telliez, J. B. MAPKAP kinase 2-deficient mice are resistant to collagen-induced arthritis. *J. Immunol.* **2006**, *177*, 1913−1917.

(16) Kotlyarov, A.; Neininger, A.; Schubert, C.; Eckert, R.; Birchmeier, C.; Volk, H. D.; Gaestel, M. MAPKAP kinase 2 is essential for LPS-induced TNF-alpha biosynthesis. *Nat. Cell Biol.* **1999**, *1*, 94−97.

(17) Anderson, D. R.; Meyers, M. J.; Vernier, W. F.; Mahoney, M. W.; Kurumbail, R. G.; Caspers, N.; Poda, G. I.; Schindler, J. F.; Reitz, D. B.; Mourey, R. J. Pyrrolopyridine inhibitors of mitogen-activated protein kinase-activated protein kinase 2 (MK-2). *J. Med. Chem.* **2007**, *50*, 2647−2654.

(18) Trujillo, J. I.; Meyers, M. J.; Anderson, D. R.; Hegde, S.; Mahoney, M. W.; Vernier, W. F.; Buchler, I. P.; Wu, K. K.; Yang, S.; Hartmann, S. J.; Reitz, D. B. Novel tetrahydro-beta-carboline-1-carboxylic acids as inhibitors of mitogen activated protein kinase-activated protein kinase 2 (MK-2). *Bioorg. Med. Chem. Lett.* **2007**, *17*, 4657−4663.

(19) Goldberg, D. R.; Choi, Y.; Cogan, D.; Corson, M.; DeLeon, R.; Gao, A.; Gruenbaum, L.; Hao, M. H.; Joseph, D.; Kashem, M. A.; Miller, C.; Moss, N.; Netherton, M. R.; Pargellis, C. P.; Pelletier, J.; Sellati, R.; Skow, D.; Torcellini, C.; Tseng, Y. C.; Wang, J.; Wasti, R.; Werneburg, B.; Wu, J. P.; Xiong, Z. Pyrazinoindolone inhibitors of MAPKAP-K2. *Bioorg. Med. Chem. Lett.* **2008**, *18*, 938−941.

(20) Kosugi, T.; Mitchell, D. R.; Fujino, A.; Imai, M.; Kambe, M.; Kobayashi, S.; Makino, H.; Matsueda, Y.; Oue, Y.; Komatsu, K.; Imaizumi, K.; Sakai, Y.; Sugiura, S.; Takenouchi, O.; Unoki, G.; Yamakoshi, Y.; Cunliffe, V.; Frearson, J.; Gordon, R.; Harris, C. J.; Kalloo-Hosein, H.; Le, J.; Patel, G.; Simpson, D. J.; Sherborne, B.; Thomas, P. S.; Suzuki, N.; Takimoto-Kamimura, M.; Kataoka, K. Mitogen-Activated Protein Kinase-Activated Protein Kinase 2 (MAPKAP-K2) as an Antiinflammatory Target: Discovery and in Vivo Activity of Selective Pyrazolo[1,5-a]pyrimidine Inhibitors Using a Focused Library and Structure-Based Optimization Approach. *J. Med. Chem.* **2012**, *55*, 6700−6715.

(21) Schlapbach, A.; Huppertz, C. Low-molecular-weight MK2 inhibitors: A tough nut to crack! *Future Med. Chem.* **2009**, *1*, 1243−1257.

(22) Mourey, R. J.; Burnette, B. L.; Brustkern, S. J.; Daniels, J. S.; Hirsch, J. L.; Hood, W. F.; Meyers, M. J.; Mnich, S. J.; Pierce, B. S.; Saabye, M. J.; Schindler, J. F.; South, S. A.; Webb, E. G.; Zhang, J.; Anderson, D. R. A Benzothiophene Inhibitor of Mitogen-Activated Protein Kinase-Activated Protein Kinase 2 Inhibits Tumor Necrosis Factor a Production and Has Oral Anti-Inflammatory Efficacy in Acute and Chronic Models of Inflammation. *J. Pharmacol. Exp. Ther.* **2010**, *333*, 797−807.

(23) Olsson, H.; Sjo, P.; Ersoy, O.; Kristoffersson, A.; Larsson, J.; Norden, B. 4-Anilino-6-phenyl-quinoline inhibitors of mitogen activated protein kinase-activated protein kinase 2 (MK2). *Bioorg. Med. Chem. Lett.* **2010**, *20*, 4738−4740.

(24) Xiaoa, D.; Zhua, X.; Sofolaridesa, M.; Degradoa, S.; Shaoa, N.; Raoa, A.; Chena, X.; Aslaniana, R.; Fossettab, J.; Tianb, F.; Trivedib, P.; Lundellb, D.; Palania, A. Discovery of a novel series of potent MK2 non-ATP competitive inhibitors using 1,2-substituted azoles as cis-amide isosteres. *Bioorg. Med. Chem. Lett.* **2014**, *24*, 3609−3613.

(25) Sullivan, J. E.; Holdgate, G. A.; Campbell, D.; Timms, D.; Gerhardt, S.; Breed, J.; Breeze, A. L.; Bermingham, A.; Pauptit, R. A.; Norman, R. A.; Embrey, K. J.; Read, J.; VanScyoc, W. S.; Ward, W. H. Prevention of MKK6-dependent activation by binding to p38alpha MAP kinase. *Biochemistry* **2005**, *44*, 16475−16490.

(26) VanScyoc, W. S.; Holdgate, G. A.; Sullivan, J. E.; Ward, W. H. Enzyme kinetics and binding studies on inhibitors of MEK protein kinase. *Biochemistry* **2008**, *47*, 5017−5027.

(27) Singh, P.; Ward, W. H. Alternative assay formats to identify diverse inhibitors of protein kinases. *Expert Opin. Drug Discovery* **2008**, *3*, 819−831.

(28) Brown, D. S.; Cumming, J. G.; Bethel, P.; Finlayson, J.; Gerhardt, S.; Nash, I.; Pauptit, R. A.; Pike, K. G.; Reid, A.; Snelson, W.; Swallow, S.; Thompson, C. The discovery of *N*-cyclopropyl-4-methyl-3-[6-(4-methylpiperazin-1-yl)-4-oxoquinazolin-3(4H)-yl]benzamide (AZD6703), a clinical p38alpha MAP kinase inhibitor for the treatment of inflammatory diseases. *Bioorg. Med. Chem. Lett.* **2012**, *22*, 3879−3883.

(29) Lukas, S. M.; Kroe, R. R.; Wildeson, J.; Peet, G. W.; Frego, L.; Davidson, W.; Ingraham, R. H.; Pargellis, C. A.; Labadia, M. E.; Werneburg, B. G. Catalysis and function of the p38 alpha.MK2a signaling complex. *Biochemistry* **2004**, *43*, 9950−9960.

(30) Cohen, P.; Alessi, D. R. Kinase drug discovery–what's next in the field? *ACS Chem. Biol.* **2013**, *8*, 96−104.

(31) Menozzi, G.; Mosti, L.; Schenone, P. Reaction of 2-dimethylaminomethylene-1,3-diones with dinucleophiles. VI. Synthesis of ethyl or methyl 1,5-disubstituted 1H-pyrazole-4-carboxylates. *J. Heterocycl. Chem.* **1987**, *24*, 1669−1675.

dx.doi.org/10.1021/jm501038s | *J. Med. Chem.* XXXX, XXX, XXX−XXX

(32) Geschwindner, S.; Dekker, N.; Horsefield, R.; Tigerström, A.; Johansson, P.; Scott, C. W.; Albert, J. S. Development of a Plate-Based Optical Biosensor Fragment Screening Methodology to Identify Phosphodiesterase 10A Inhibitors. *J. Med. Chem.* **2013**, *56*, 3228−3234.
(33) ter Haar, E.; Prabhakar, P.; Liu, X.; Lepre, C. Crystal structure of the p38 alpha-MAPKAP kinase 2 heterodimer. *J. Biol. Chem.* **2007**, *282*, 9733−9739.
(34) White, A.; Pargellis, C. A.; Studts, J. M.; Werneburg, B. G.; Farmer, B. T., 2nd Molecular basis of MAPK-activated protein kinase 2:p38 assembly. *Proc. Natl. Acad. Sci. U. S. A.* **2007**, *104*, 6353−6358.
(35) The coordinates have been deposited in the PDB with accession codes 4TYK for compound **6** and 4TYH for compound **12**.
(36) Michelotti, E. L.; Moffett, K. K.; Nguyen, D.; Kelly, M. J.; Shetty, R.; Chai, X.; Northrop, K.; Namboodiri, V.; Campbell, B.; Flynn, G. A.; Fujimoto, T.; Hollinger, F. P.; Bukhtiyarova, M.; Springman, E. B.; Karpusas, M. Two classes of p38α MAP kinase inhibitors having a common diphenylether core but exhibiting divergent binding modes. *Bioorg. Med. Chem. Lett.* **2005**, *15*, 5274−5279.
(37) Das, J.; Moquin, R. V.; Dyckman, A. J.; Li, T.; Pitt, S.; Zhang, R.; Shen, D. R.; McIntyre, K. W.; Gillooly, K.; Doweyko, A. M.; Newitt, J. A.; Sack, J. S.; Zhang, H.; Kiefer, S. E.; Kish, K.; McKinnon, M.; Barrish, J. C.; Dodd, J. H.; Schieven, G. L.; Leftheris, K. 5-Amino-Pyrazoles as Potent and Selective P38alpha Inhibitors. *Bioorg. Med. Chem. Lett.* **2010**, *20*, 6886−6889.
(38) *Molecular Operating Environment (MOE)*, 2013.08. Chemical Computing Group Inc., 1010 Sherbooke St. West, Suite #910, Montreal, QC, Canada, H3A 2R7.
(39) Crawley, G. C.; Hennequin, L. F. A.; Lambert, C. M.-P.; McKerrecher, D.; Plé, P.; Poyser, J. P. International PatentWO0104102, 2001.
(40) Hohwy, M. unpublished results.
(41) Vogtherr, M.; Saxena, K.; Grimme, S.; Betz, M.; Schieborr, U.; Pescatore, B.; Langer, T.; Schwalbe, H. NMR backbone assignment of the mitogen-activated protein (MAP) kinase p38. *J. Biomol. NMR* **2005**, *32*, 175.
(42) Winn, M. D.; Ballard, C. C.; Cowtan, K. D.; Dodson, E. J.; Emsley, P.; Evans, P. R.; Keegan, R. M.; Krissinel, E. B.; Leslie, A. G.; McCoy, A.; McNicholas, S. J.; Murshudov, G. N.; Pannu, N. S.; Potterton, E. A.; Powell, H. R.; Read, R. J.; Vagin, A.; Wilson, K. S. Overview of the CCP4 suite and current developments. *Acta Crystallogr., Sect. D: Biol. Crystallogr.* **2011**, *67*, 235−242.
(43) Emsley, P.; Lohkamp, B.; Scott, W. G.; Cowtan, K. Features and development of Coot. *Acta Crystallogr., Sect. D: Biol. Crystallogr.* **2010**, *66*, 486−501.
(44) Murshudov, G. N.; Vagin, A. A.; Dodson, E. J. Refinement of macromolecular structures by the maximum-likelihood method. *Acta Crystallogr., Sect. D: Biol. Crystallogr.* **1997**, *53*, 240−255.

■ NOTE ADDED AFTER ASAP PUBLICATION

After this paper was published ASAP on October 9, 2014, a correction was made to Table 2. The corrected version was reposted October 17, 2014.